© 2020. Published by The Company of Biologists Ltd | Journal of Cell Science (2020) 133, jcs246710. doi:10.1242/jcs.246710

RESEARCH ARTICLE

Neuronal MT1-MMP mediates ECM clearance and Lrp4 cleavage for agrin deposition and signaling in presynaptic development

Marilyn Janice Oentaryo, Anna Chung-Kwan Tse and Chi Wai Lee*

ABSTRACT

Agrin is a crucial factor that induces postsynaptic differentiation at neuromuscular junctions (NMJs), but how secreted agrin is locally deposited in the context of extracellular matrix (ECM) environment and its function in presynaptic differentiation remain largely unclear. Here, we report that the proteolytic activity of neuronal membrane-type 1 matrix metalloproteinase (MT1-MMP; also known as MMP14) facilitates agrin deposition and signaling during presynaptic development at NMJs. Firstly, agrin deposition along axons exhibits a time-dependent increase in cultured neurons that requires MMP-mediated focal ECM degradation. Next, local agrin stimulation induces the clustering of mitochondria and synaptic vesicles, two well-known presynaptic markers, and regulates vesicular trafficking and surface insertion of MT1-MMP. MMP inhibitor or MT1-MMP knockdown suppresses agrin-induced presynaptic differentiation, which can be rescued by treatment with the ectodomain of low-density lipoprotein receptor-related protein 4 (Lrp4). Finally, neuronal MT1-MMP knockdown inhibits agrin deposition and nerve-induced acetylcholine receptor clustering in nerve-muscle co-cultures and affects synaptic structures at *Xenopus* NMJs *in vivo*. Collectively, our results demonstrate a previously unappreciated role of agrin, as well as dual functions of neuronal MT1-MMP proteolytic activity in orchestrating agrin deposition and signaling, in presynaptic development.

KEY WORDS: Agrin, Extracellular matrix, Matrix metalloproteinase, Presynaptic differentiation, Lrp4

INTRODUCTION

The construction of neuronal circuit involves an intricate array of connections to be established during early development that allows the formation and proper functioning of the nervous system (Sanes and Yamagata, 2009; Yogev and Shen, 2014). Generally, neuronal outgrowth and synaptogenesis are considered as two distinct phases in neuronal circuit wiring (Dai and Peng, 1996; Peng et al., 2003). During the early stage of wiring, the growth cone, a motile structure located at the leading edge of a growing axon, extends and navigates the axon outward to the target cell. Binding of the extracellular ligands to their receptors on the plasma membrane triggers intracellular signaling pathways to regulate the motility, outgrowth and turning response of the growth cones (Lowery and Van Vactor, 2009; Omotade et al., 2017). After reaching a specific target, the motile growth cone structure then transforms into a much more stable nerve terminal for activity-dependent neurotransmitter release. This is evidenced by the accumulation of synaptic vesicle (SV) and mitochondrial clusters, two of the most prominent presynaptic differentiation markers (Dai and Peng, 1998; Lee and Peng, 2006). However, whether the transition from neuronal outgrowth to synaptogenic phase is regulated by intrinsic or extrinsic factors, and their underlying molecular mechanisms remain largely unclear.

Agrin, a large heparan sulfate proteoglycan (HSPG), has been well characterized for its functions in postsynaptic differentiation at developing neuromuscular junctions (NMJs) (Li et al., 2018; Ruegg and Bixby, 1998). Agrin induces the clustering of acetylcholine receptors (AChRs) in muscle fibers through the activation of low-density lipoprotein receptor-related protein 4 (Lrp4) and muscle-specific kinase (MuSK) signaling pathway (Kim et al., 2008; Zhang et al., 2008). At the tripartite NMJs, agrin is expressed in and secreted by all three cell types (i.e. motor neurons, muscle fibers and perisynaptic Schwann cells) (Reist et al., 1992; Yang et al., 2001). However, the multiple alternatively spliced forms of agrin have different binding characteristics and bioactivities (Scotton et al., 2006). While motor neurons express a mixture of agrin isoforms, those isoforms containing inserts of four and eight amino acids at site A and B, respectively, are the most effective in inducing AChR clustering *in vitro* and *in vivo* (Bezakova et al., 2001; Gesemann et al., 1995). In contrast to the well-characterized functions of agrin in postsynaptic differentiation at NMJs, the regulation of agrin deposition by spinal neurons and the physiological function of endogenous agrin in presynaptic differentiation, however, are still elusive.

The extracellular matrix (ECM) contains different ligands, such as laminin, collagen and fibronectin, that modulate the adhesion and motility of neuronal growth cones (Kerstein et al., 2015). Interestingly, neuronal growth cones are associated with the activity of matrix metalloproteinases (MMPs) to mediate local proteolysis of ECM proteins, which may spatiotemporally control the release of ECM-associated growth factors (Santiago-Medina et al., 2015). Currently, 23 different MMPs have been identified in humans, which differ in their substrate specificity (Nagase et al., 2006), and they are classified as either membrane-bound or soluble forms. Membrane-type 1 MMP (MT1-MMP, also known as MMP14), can degrade a range of different ECM components (collagen, gelatin and laminin) (Itoh, 2015) and activate other soluble MMPs through proteolytic cleavage of their pro-domain peptide (Deryugina et al., 2001; Li et al., 2017). However, whether MMP-mediated proteolytic regulation of ECM proteins and/or other synaptogenic factors affects presynaptic development remains to be investigated.

In this study, we investigated how secreted agrin is locally deposited in the context of ECM environment through the action of MT1-MMP that induces presynaptic development. Firstly, we show that agrin deposition along the neurites can be strongly detected in

School of Biomedical Sciences, Li Ka Shing Faculty of Medicine, The University of Hong Kong, Hong Kong.

*Author for correspondence (chiwai.lee@hku.hk)

M.J.O., 0000-0002-1798-3379; C.W.L., 0000-0003-4619-3189

Handling Editor: Michael Way
Received 24 March 2020; Accepted 16 June 2020

Journal of Cell Science (2020) 133, jcs246710. doi:10.1242/jcs.246710

1- or 2-day-old *Xenopus* spinal neuron cultures, but not in young cultures at which the neuronal outgrowth phase is dominant. MMP-mediated ECM degradation allows the spatial deposition of agrin along the neurites. We further demonstrate that the application of polystyrene beads coated with recombinant neural agrin proteins focally induces presynaptic differentiation in cultured spinal neurons, as reflected by a panel of different presynaptic markers, through Lrp4-dependent mechanisms. Next, we identify that endogenous MT1-MMP is required for ECM degradation along the neurites and agrin bead-induced presynaptic differentiation. Time-lapse imaging further shows the dynamic axonal transport of MT1-MMP vesicles, followed by the local capture and surface delivery of vesicular MT1-MMP proteins at the agrin bead-contacted sites. Furthermore, either pharmacological inhibition of MMP activity or reduced expression of endogenous MT1-MMP suppresses agrin-induced presynaptic differentiation, and the inhibitory effects can be rescued by treatment with the ectodomain of Lrp4 (ecto-Lrp4), suggesting another function of MT1-MMP in Lrp4 proteolytic activation. Finally, we show that neuronal MT1-MMP plays an essential role in early NMJ formation *in vitro* and *in vivo*. In summary, this study has identified a previously unappreciated role of agrin in presynaptic differentiation and a dual regulatory role of MT1-MMP in orchestrating agrin deposition and signaling through ECM degradation and Lrp4 activation, respectively.

RESULTS

Intrinsic neuronal mechanisms control the transition from axonal growth to synaptogenesis

It has been suggested that neuronal development consists of two distinct phases: neuronal outgrowth and synaptogenesis (Dai and Peng, 1996; Peng et al., 2003). After plating dissociated *Xenopus* spinal neurons on ECM-coated substratum for 4–8 h, the neuronal outgrowth phase is dominant, as demonstrated by the presence of axonal growth cones, the motile structures located at the tips of growing axons, in these young neurons (Fig. 1A). As the cultures became older, a gradual reduction in neuronal outgrowth, as reflected by the reduced length of axonal extension, was observed (Fig. 1A,B). To examine whether the outgrowth and synaptogenic phases of spinal neurons are developmentally regulated in culture, we next examined the secretion and deposition of agrin, a crucial nerve-derived factor for inducing postsynaptic differentiation, in cultured neurons at different time points. While agrin deposition was seldom detected in the outgrowing young neurons, we started to detect agrin deposition, together with a gradual increase in the intensity of agrin immunostaining signals, to be associated with most neurites in the older neurons (Fig. 1C). By examining the patterns of fluorescent gelatin conjugate, the ECM protein used for substratum coating, we intriguingly detected an increasing extent of gelatin degradation that was spatially and temporally correlated with the patterns of agrin deposition in older (i.e. 1- or 2-day-old) neurons (arrows in Fig. 1C). Line profiles of fluorescent gelatin, and agrin and synapsin 1 immunostaining signals further demonstrated that the segment of neurite with reduced fluorescent gelatin intensity was closely associated with increased signals of agrin and synapsin 1; by contrast, the segment of the same neurite with basal fluorescent gelatin intensity was closely associated with the portion where there was minimal signals of agrin and synapsin 1 in 1-day-old cultures (Fig. 1D). Notably, expression and deposition of endogenous agrin were strongly detected along the entire length of neurites with extensive ECM degradation in 2-day-old cultures (bottom row, Fig. 1C). Quantification showed a time-dependent increase in the percentage of neurites with gelatin degradation, and the extent of degradation, after cell plating in culture over time (Fig. 1E). A similar trend was also observed in the percentage of neurites with agrin deposition and its fluorescence intensity in the cultured neurons at different time points (Fig. 1F), which was also coupled with an increased intensity of synapsin 1 (Fig. 1G), a highly conserved phosphoprotein involved in the regulation of neurotransmitter release (Greengard et al., 1987). When we performed the ECM degradation assay using another ubiquitously expressed ECM protein, collagen, we also detected a strong spatial correlation between synapsin 1 localization and focal degradation of fluorescent collagen at different segments of the same neurite in 1-day-old cultures (Fig. S1). These results suggest that local degradation of ubiquitously expressed ECM proteins is required for the proper deposition and localization of agrin at the nascent synaptic basal lamina, which may be crucial developmentally regulated cellular events in presynaptic development.

Agrin is a molecular switch from axonal growth to presynaptic differentiation in young neurons

Since neuronal growth cones translate environmental signals into directional guidance responses for the extending axons to find their ultimate destination (Lowery and Van Vactor, 2009), we anticipated that the transition of neuronal outgrowth to synaptogenic phase could be reflected by the morphological changes in growth cone structures. By comparing the growth cone morphology in cultured neurons at different time points, we observed a developmental shift from the normal fan-shaped to the collapsed bulb-shaped growth cone structures between young (4–8 h) and old (1 day) neurons (Fig. 2A). In the old neurons, collapsed growth cone structures were found in >70% of the neurites, as compared to only ∼20% showing such structures in the young neurons (Fig. 2B), implicating a gradual loss of axonal growth ability of spinal neurons in culture over time. Interestingly, bath treatment of recombinant agrin, at 0.1 mg/ml, significantly induced growth cone collapse in the young neurons, but not in the old neurons. Together with growth cone collapse, we also detected a significant reduction in neurite extension in the young neurons treated with agrin (Fig. 2C). To determine the effects of agrin treatment on presynaptic differentiation, we next examined the clustering of SVs and mitochondria, both of which are well-known presynaptic markers that are enriched in nerve terminals and varicosities in cultured neurons (Dai and Peng, 1995; Lee and Peng, 2006). Compared to the untreated cultures, agrin treatment significantly increased SV and mitochondrial clustering along the neurites in the young neurons (Fig. 2D–F). However, no further increase was observed in the old neurons after agrin treatment, suggesting that expression and deposition of endogenous agrin are sufficient to induce presynaptic differentiation in the old neurons. Notably, agrin treatment caused a significant increase in the intensity of MitoTracker signals (Fig. 2E), indicating that the membrane potential and ATP generating ability of mitochondria were elevated by agrin treatment in these young neurons.

To further determine whether agrin expression and/or deposition are developmentally regulated processes that serve as a stop signal for the transition from the neuronal outgrowth to synaptogenic phase in culture, we manipulated agrin expression and activity by means of an antisense morpholino oligonucleotide (MO) and functional blocking antibody, respectively. As no commercial antibodies were available to detect *Xenopus* agrin by western blotting, the knockdown efficiency of agrin MO was validated by immunostaining, with a 57% reduction in endogenous agrin protein level seen as compared to the control (Fig. S2). In 1-day-old

Journal of Cell Science (2020) 133, jcs246710. doi:10.1242/jcs.246710

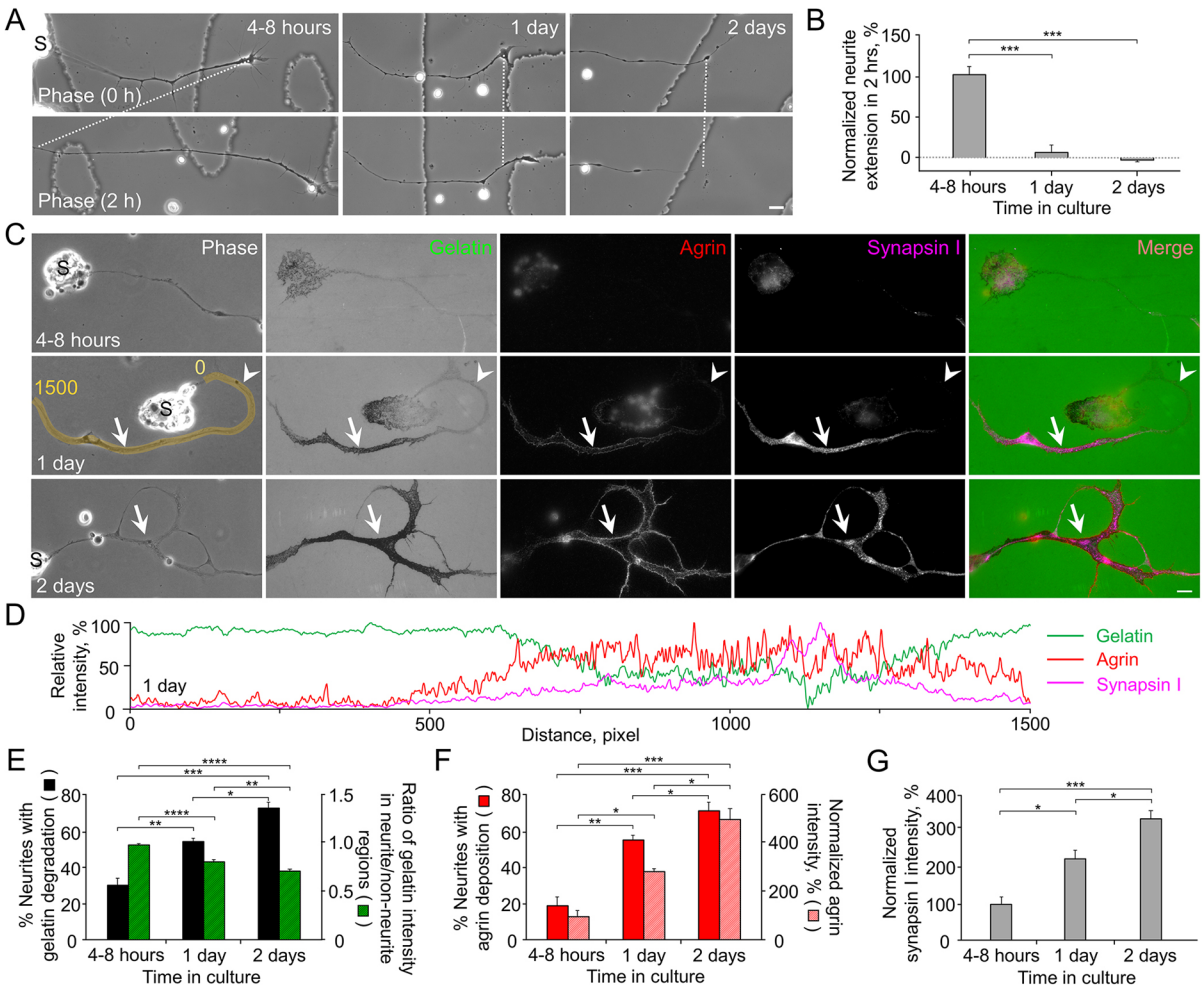

Fig. 1. Cultured spinal neurons exhibit time-dependent change in ECM degradation, agrin deposition and synapsin 1 localization along the neurites. (A) Representative images showing the extension length of cultured *Xenopus* spinal neurons at different time points. Dotted lines align different images based on the position of growth cones at the first time point. S, soma. (B) Quantitative analysis showing the normalized net length of neurite extension after 2 h in cultured neurons at different time points. *n*=85 neurites in each experimental group from three independent experiments. (C) Representative images showing the patterns of fluorescent gelatin degradation, agrin deposition and synapsin 1 localization along neurites in cultured spinal neurons at different time points. Arrows indicate the segment of a neurite with both gelatin degradation and localized signals of agrin and synapsin 1; arrowheads indicate the absence or minimal levels of gelatin degradation, agrin deposition, and synapsin 1 localization at the other segment of the same neurite. The yellow line indicates the region of interest for generating line profiles along the length of neurites, with the numbers representing the relative position in pixels. (D) Line profiles showing the relative fluorescent intensities of gelatin, agrin and synapsin 1 along the yellow line (indicated in C) in a 1-day-old cultured neuron. (E–G) Quantitative analysis showing the increasing percentage of neurites with gelatin degradation (solid bars) and the extent of gelatin degradation (patterned bars) (E), the increasing percentage of neurites with agrin deposition (solid bars), the increasing intensity of agrin immunostaining signals (patterned bars) (F), and the increasing intensity of synapsin 1 (G) in cultured neurons over time. For quantifying the percentage, *n*=150 neurites were measured in each experimental group from three independent experiments. For quantifying the intensity, *n*=65 (4-8 h), 65 (1 day), or 52 (2 days) neurites were measured from three independent experiments. Data are mean±s.e.m. **P*<0.05; ***P*<0.01; ****P*<0.001; *****P*<0.0001 (one-way ANOVA with Tukey's multiple comparison test). Scale bars: 10 µm.

cultures, agrin knockdown or the antibody-treated neurons remained in the outgrowth phase, as reflected by a significant increase in neurite extension and reduced percentage of collapsed growth cones, compared with the control neurons (Fig. 2G–I). We found that recombinant agrin treatment was able to rescue the effects on neurite extension and growth cone structures caused by agrin knockdown, but not by anti-agrin functional blocking antibody. Intriguingly, semi-quantitative reverse-transcription polymerase chain reaction (RT-PCR) data showed that agrin mRNA levels were comparable between young and old neurons (Fig. S3). Together, our data suggest that an intrinsic developmental regulation of agrin secretion and deposition, and not its expression, may serve as a molecular switch from neuronal outgrowth to presynaptic differentiation in culture.

Local application of agrin induces presynaptic differentiation through neuronal Lrp4

Previous studies have shown that local application of synaptogenic factors, such as basic fibroblast growth factor (bFGF), via polystyrene beads can spatio-temporally induce presynaptic differentiation, as reflected by the clustering of SVs and mitochondria at the bead–neurite contact sites (Lee and Peng, 2006, 2008). While agrin-coated beads have been found to be effective in inducing postsynaptic AChR clustering in cultured muscle cells, as shown in our previous study (Lee et al., 2009), here we further tested whether agrin beads can spatiotemporally induce presynaptic differentiation to a similar extent to bFGF beads in spinal neurons cultured for less than 1 day. After adding agrin- or

Journal of Cell Science (2020) 133, jcs246710. doi:10.1242/jcs.246710

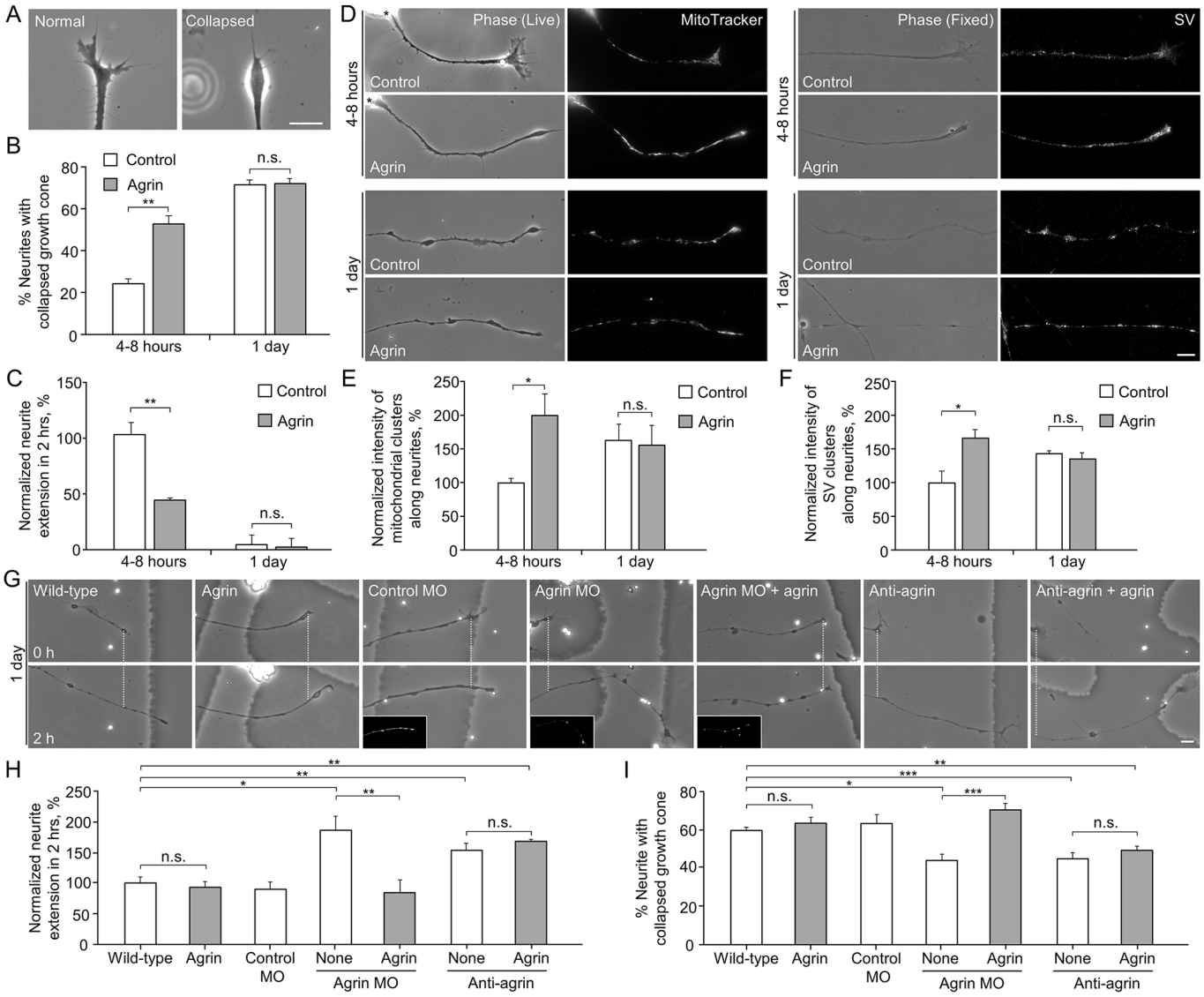

Fig. 2. Bath treatment with agrin suppresses neuronal outgrowth and promotes the clustering of presynaptic markers in young cultured spinal neurons. (A) Representative images showing the morphological difference between a normal and collapsed growth cone in cultured *Xenopus* spinal neurons. (B) Quantitative analysis showing that bath application of agrin significantly induces growth cone collapse in young neurons, but not in old neurons. *n*=150 neurites in each experimental group from three independent experiments. (C) Quantitative analysis showing that agrin treatment significantly inhibits axonal growth in young neurons. *n*=85 neurites in each experimental group from three independent experiments. (D) Representative images showing that agrin treatment significantly increases mitochondrial and SV clustering along the neurites in young neurons, but not in old neurons. Asterisks indicate the soma. (E,F) Quantitative analysis showing the effects of agrin treatment on the intensity of mitochondrial clusters (E) and SV clusters (F) along the neurites in young versus old cultures. *n*=60 neurites in each experimental group from three independent experiments. (G) Representative images showing the effects on neurite extension upon molecular knockdown with agrin MO or treatment with anti-agrin functional blocking antibody. Dotted lines align different images based on the position of growth cones at the first time point. Insets indicate the fluorescent dextran signals. (H) Quantitative analysis showing the effects of agrin knockdown or inhibition on neurite extension. *n*=264 (wild-type), 303 (agrin), 202 (control MO), 185 (agrin MO), 201 (agrin MO+agrin), 173 (anti-agrin), or 224 (anti-agrin+agrin) neurites from at least three independent experiments. (I) Quantitative analysis showing the effects of agrin knockdown or inhibition on growth cone collapse. *n*=200 (wild-type or agrin) or 150 (other experimental groups) neurites from at least three independent experiments. Data are mean±s.e.m. **P*<0.05; ***P*<0.01; ****P*<0.001; n.s., not significant (unpaired Student's *t*-test). Scale bars: 10 µm.

bFGF-coated beads to these young spinal neurons for 4 h, we detected the accumulation of SV and mitochondrial clusters at most of the bead–neurite contact sites (Fig. 3A). Specifically, the effectiveness of agrin-coated beads for inducing the clustering of these two presynaptic markers was comparable to that of bFGF-coated beads (Fig. 3B). In contrast, BSA control beads were found to be ineffective. The loading and unloading experiments with the lipophilic styryl dye FM1-43 indicated that agrin beads could induce the clustering of readily releasable SVs at the bead–neurite contacts in live cultured spinal neurons (Fig. 3C). Furthermore, fluorescent phalloidin staining and phosphotyrosine, bassoon, and piccolo immunostaining showed that filamentous actin (F-actin) scaffold (Peng, 1983), tyrosine-phosphorylated presynaptic proteins (Dai and Peng, 1995) and active zone markers (Zhai et al., 2001) were all highly enriched at agrin bead–neurite contacts (Fig. 3D). These findings strongly support the hypothesis that localized agrin stimulation is capable of inducing the assembly of various presynaptic components for

Journal of Cell Science (2020) 133, jcs246710. doi:10.1242/jcs.246710

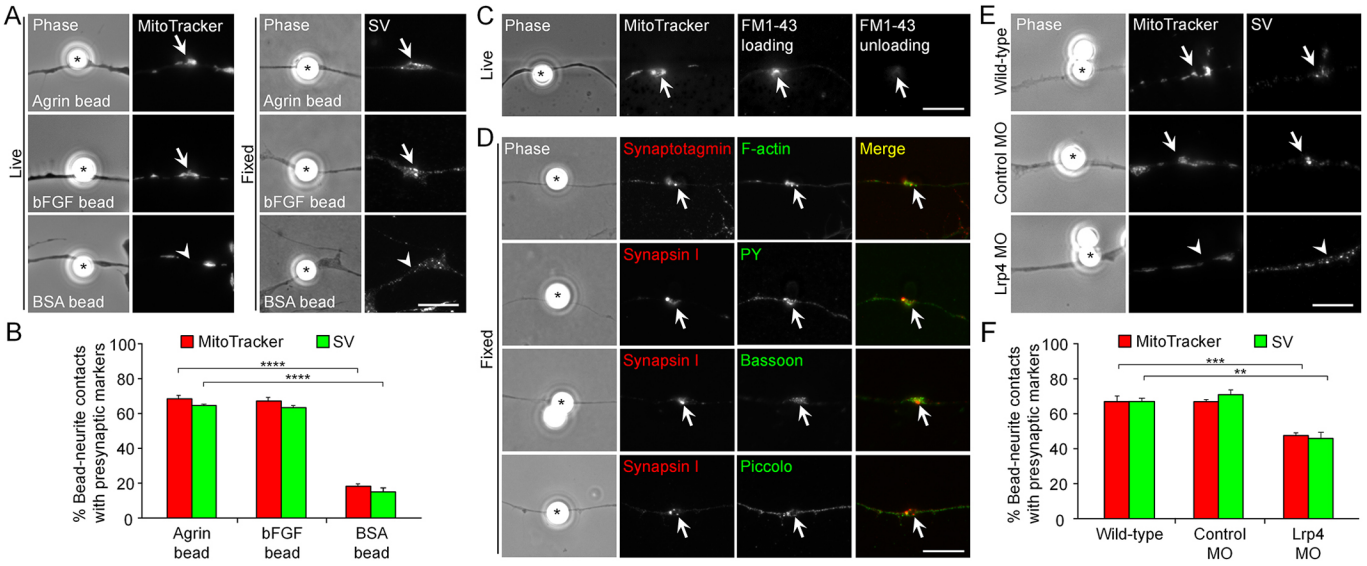

Fig. 3. Local agrin stimulation induces presynaptic differentiation through an Lrp4-dependent pathway. (A) Representative images showing the localization of mitochondrial and SV clusters at the sites of neurite in contact with agrin- or bFGF-coated beads, but not with BSA control beads. (B) Quantitative analysis showing that agrin beads effectively induce mitochondrial and SV clusters to an extent comparable to bFGF-coated beads. *n*=150 bead–neurite contacts in each experimental group from three independent experiments. (C) Representative images showing that agrin beads induce the clustering of the readily releasable pool of SVs, as revealed by the sequential loading and unloading of FM1-43 in high potassium solution. (D) Representative images showing the enrichment of F-actin, tyrosine phosphorylated (PY) presynaptic proteins and active zone proteins at bead–neurite contacts. (E) Representative images showing the requirement of neuronal Lrp4 for agrin-induced presynaptic differentiation. (F) Quantitative analysis showing the inhibitory effects of Lrp4 knockdown on agrin-induced presynaptic differentiation. *n*=150 bead–neurite contacts in each experimental group from three independent experiments. Asterisks indicate the bead–neurite contact sites; arrows indicate the localization of presynaptic markers; arrowheads indicate the absence of presynaptic marker localization at the bead–neurite contacts. Data are mean±s.e.m. ***P*<0.01, ****P*<0.001, *****P*<0.0001 (one-way ANOVA with Dunnett's multiple comparison test).

neurotransmitter release. Since the effectiveness of agrin beads on the clustering of SVs and mitochondria was comparable in either young or old neurons (Fig. S4), old neurons were primarily used in our subsequent experiments as they had much longer neurites for making bead contacts.

Since a role for the agrin–Lrp4-–MuSK signaling pathway has been well characterized in postsynaptic differentiation at NMJs (Kim et al., 2008; Zhang et al., 2008), we next investigated whether agrin bead-induced presynaptic differentiation also requires neuronal Lrp4 expression. Lrp4 mRNA and proteins were detected in cultured *Xenopus* spinal neurons, as shown by RT-PCR and immunostaining data (Fig. S5A,B). To determine the requirement of Lrp4 for presynaptic differentiation, endogenous Lrp4 expression was knocked down by an antisense MO and fluorescent dextran was used as the cell lineage tracer for identifying the MO-containing neurons in early *Xenopus* embryos. Since there were no commercial antibodies available for detecting *Xenopus* Lrp4 by western blotting, we performed immunostaining experiments, which showed a significant reduction of endogenous Lrp4 signals, by 62%, in Lrp4 MO neurons (Fig. S5C,D). Importantly, Lrp4 knockdown significantly inhibited agrin bead-induced clustering of mitochondria and SVs compared with that seen in the wild-type neurons or neurons with control MO (Fig. 3E,F). These results suggest that neuronal Lrp4 expression is required for agrin-induced presynaptic differentiation.

MT1-MMP activity regulates agrin-induced presynaptic differentiation

Recent studies have suggested that MMP-mediated ECM degradation regulates axonal guidance of neuronal growth cones (Santiago-Medina et al., 2015); however, whether MMP activity also regulates the development of presynaptic nerve terminals remains unclear. To test this, we first used a broad-spectrum MMP inhibitor BB-94, at 5 µM, which caused a complete inhibition in the degradation of fluorescent gelatin associated with the cultured neurons (Fig. 4A,B). Moreover, BB-94 treatment significantly suppressed agrin deposition and synapsin 1 localization along the neurites (Fig. 4C,D), further supporting the notion that ECM degradation is a prerequisite for the proper deposition and localization of secreted agrin to induce presynaptic differentiation.

To address whether agrin can be proteolytically degraded by MMP activity, we then performed agrin immunostaining, followed by live-cell imaging, to examine the effects of BB-94 treatment on the fluorescence intensity of secreted agrin signals. Agrin immunostaining signals were found to be comparable in the presence or absence of BB-94 after 1 day (Fig. 4E,F), suggesting that agrin is not a proteolytic target of MMPs in spinal neurons. Importantly, BB-94 treatment was found to significantly inhibit agrin bead-induced presynaptic differentiation (Fig. 4G), as reflected by a reduced percentage of bead–neurite contacts with mitochondrial or SV clusters (Fig. 4H) and a lower fluorescence intensity of these two presynaptic markers at the bead–neurite contacts (Fig. 4I). These data suggest that MMP proteolytic activity, on top of its known function in ECM degradation, may regulate other signaling molecule(s) required for presynaptic differentiation.

MT1-MMP is the best-characterized and prevalent isoform among the 23 known MMPs in humans. We next examined whether MT1-MMP is required for agrin-induced presynaptic differentiation by an MO-mediated knockdown approach. The knockdown efficiency of the MT1-MMP MO in *Xenopus* embryos was validated by western blot analysis in our recent study (Chan et al., 2020a). In cultured spinal neurons, the specificity of MT1-MMP antibody was further demonstrated by a positive correlation

Journal of Cell Science (2020) 133, jcs246710. doi:10.1242/jcs.246710

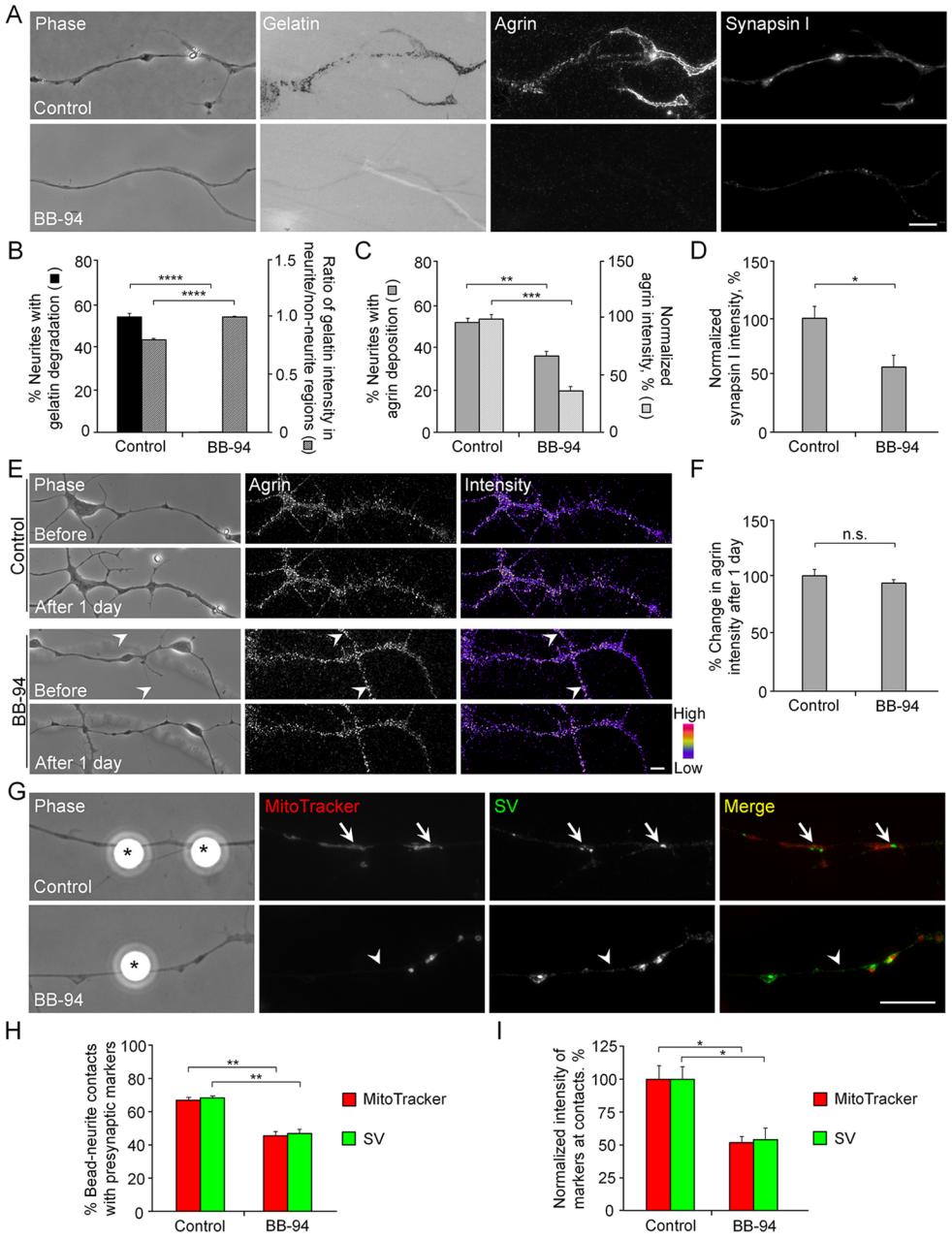

Fig. 4. MMP proteolytic activity regulates agrin-induced presynaptic differentiation. (A) Representative images showing that the broad-spectrum MMP inhibitor BB-94 completely inhibits gelatin degradation associated with neurites, and significantly suppresses agrin deposition and synapsin 1 localization in 1-day-old cultured neurons. (B–D) Quantitative analysis showing the suppression of fluorescent gelatin degradation (B), inhibition of agrin deposition (C) and reduction of synapsin 1 intensity (D) upon BB-94 treatment. For quantifying the percentage, *n*=150 neurites in each experimental group were measured from three independent experiments. For quantifying the intensity, *n*=65 (control) or 66 (BB-94) neurites were measured from three independent experiments. (E) Representative images showing no significant change in the fluorescence intensity of secreted agrin in response to BB-94 treatment for 1 day. Arrowheads indicate the signals of secreted agrin from a previously retracted neurite. (F) Quantitative analysis showing the percentage change in agrin intensity before and after BB-94 treatment. *n*=43 (control) or 48 (BB-94) neurites from three independent experiments. (G) Representative images showing the inhibitory effects of BB-94 on mitochondrial and SV clustering induced by agrin beads. Asterisks indicate the bead–neurite contact sites. Arrows and arrowheads indicate the presence and absence of presynaptic marker localization at the bead–neurite contacts, respectively. (H) Quantitative analysis showing the effects of BB-94 on the clustering of presynaptic markers at agrin bead–neurite contacts. *n*=150 bead–neurite contacts in each experimental group from three independent experiments. (I) Quantitative analysis showing the effects of BB-94 on the fluorescence intensity of the presynaptic markers at agrin bead–neurite contacts. *n*=60 bead–neurite contacts in each experimental group from three independent experiments. Data are mean±s.e.m. **P*<0.05; ***P*<0.01; ****P*<0.001; *****P*<0.0001; n.s., not significant (unpaired Student's *t*-test). Scale bars: 10 µm.

between the fluorescence intensity of endogenous MT1-MMP signals in different neurites and the extent of fluorescent gelatin degradation associated with those neurites (Fig. S6A,B). In MT1-MMP MO neurons, a significant inhibition of fluorescent gelatin degradation associated with the neurites was detected (Fig. 5A,B), which was contributed to by a reduced endogenous

Journal of Cell Science (2020) 133, jcs246710. doi:10.1242/jcs.246710

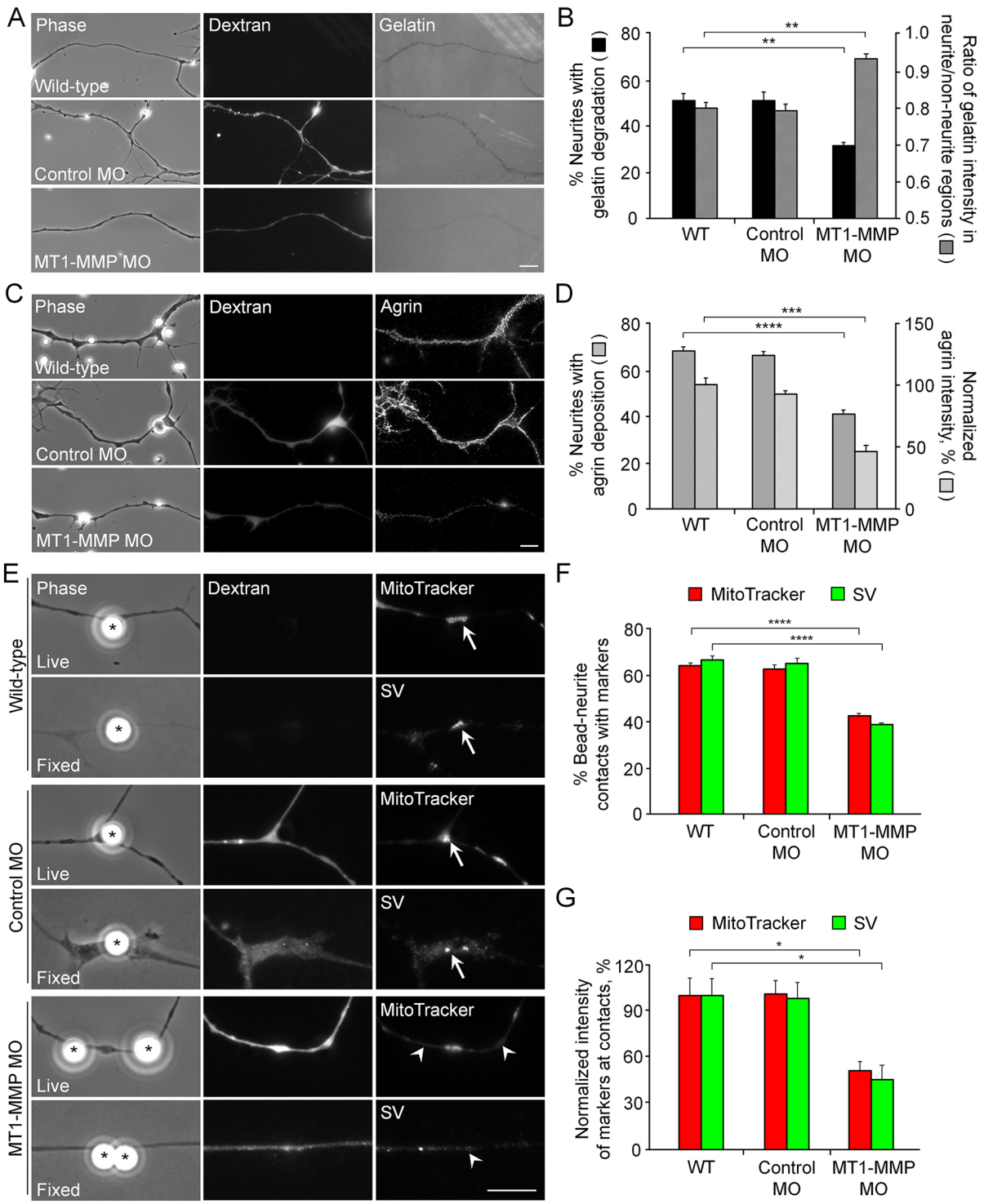

Fig. 5. MT1-MMP is required for agrin-induced presynaptic differentiation. (A) Representative images showing the reduction of gelatin degradation associated with MT1-MMP knockdown neurons. Fluorescent dextran indicates the presence of microinjected MO in cultured neurons. (B) Quantitative analysis showing that MO-mediated MT1-MMP knockdown reduces the percentage of neurites with gelatin degradation (solid bars) and the extent of gelatin degradation (patterned bars). (C) Representative images showing the reduction of agrin deposition associated with MT1-MMP knockdown neurons. Fluorescent dextran indicates the presence of microinjected MO in cultured neurons. (D) Quantitative analysis showing that MO-mediated MT1-MMP knockdown reduces the percentage of neurites with agrin deposition (solid bars) and the intensity of secreted agrin (patterned bars). (E) Representative images showing that MO-mediated MT1-MMP knockdown inhibits agrin bead-induced clustering of mitochondria and SVs in live and fixed cultured neurons, respectively. Fluorescent dextran indicates the presence of microinjected MO in cultured neurons. Asterisks indicate the bead–neurite contact sites. Arrows and arrowheads indicate the presence and absence of presynaptic marker localization at the bead–neurite contacts, respectively. (F,G) Quantitative analysis showing that MT1-MMP knockdown reduces the percentage of agrin bead–neurite contacts with mitochondrial and SV clusters (F) and their intensities at the bead–neurite contacts (G). Data are mean±s.e.m. For quantifying the percentage, n=150 neurites in each experimental group were measured from three independent experiments. For quantifying the intensity, n=30 neurites in each experimental group were measured from three independent experiments. *P<0.05; **P<0.01; ***P<0.001; ****P<0.0001 (one-way ANOVA with Dunnett's multiple comparison test). Scale bars: 10 µm.

Journal of Cell Science (2020) 133, jcs246710. doi:10.1242/jcs.246710

MT1-MMP expression level (Fig. S6C,D). As MT1-MMP-mediated ECM degradation is required for agrin deposition, we also detected a significant reduction of agrin immunostaining signals in MT1-MMP MO neurons, as expected (Fig. 5C,D). Importantly, agrin bead-induced presynaptic differentiation was significantly suppressed in MT1-MMP MO neurons (Fig. 5E), as reflected by a reduced percentage of bead–neurite contacts with mitochondrial or SV clusters and a lower fluorescence intensity of those two presynaptic markers at the bead–neurite contacts compared to that in the wild-type or control MO neurons (Fig. 5F, G). Taken together, these data demonstrated that endogenous MT1-MMP expression is required not only for agrin deposition through mediating ECM degradation, but also for agrin signaling involved in presynaptic differentiation.

MT1-MMP trafficking and surface insertion are spatiotemporally targeted to agrin bead-stimulated sites

Similar to endogenous MT1-MMP localization, exogenous MT1-MMP–mCherry signals were found along the entire neurites but with a preferential enrichment at the varicosities (Fig. 6A), the specialized structures containing clusters of SVs, dense-core vesicles and mitochondria (Lee and Peng, 2006; Peng et al., 1987). After agrin bead stimulation, spatial localizations of both endogenous MT1-MMP and exogenous MT1-MMP–mCherry signals were detected at the bead–neurite contact sites (Fig. 6B), suggesting that MT1-MMP–mCherry overexpression did not alter the localization patterns of MT1-MMP in cultured neurons.

Since MT1-MMP is an integral membrane protein, its proteolytic activity requires the intracellular trafficking of MT1-MMP vesicles to the sites of agrin bead stimulation in a spatially and temporally controlled manner. To test this, we performed live-cell imaging to track the mobility of MT1-MMP–mCherry signals along the neurites after agrin bead stimulation. While MT1-MMP–mCherry signals were found to be highly enriched at agrin bead–neurite contact sites (Fig. 6C, arrows), these MT1-MMP–mCherry vesicles were relatively immobile, as reflected by the white-colored signals in a merge image of three different time-points (0, 10 and 20 s) and by the largely straight vertical lines in the kymograph (Fig. 6C, bottom panel). In contrast, other MT1-MMP–mCherry signals along the neurites outside the bead contacts were relatively motile, exhibiting bidirectional movement along the neurites.

To further determine whether MT1-MMP–mCherry vesicles are locally captured at the bead–neurite contact, we next performed fluorescence recovery after photobleaching (FRAP) experiments to track the mobility of MT1-MMP–mCherry vesicles before and after passing through the bead-contacted sites (Fig. 6D). Before photobleaching, immobile MT1-MMP–mCherry signals were locally enriched at the bead–neurite contact (Fig. 6E, left column, arrows). Then, a region of the bead–neurite contact site containing MT1-MMP–mCherry signals (dotted square region in Fig. 6D) was photobleached and followed by performing time-lapse imaging to visualize the dynamic movement of MT1-MMP–mCherry vesicles into the photobleached region. To illustrate the temporal movement of MT1-MMP vesicles, MT1-MMP–mCherry signals from three different time-points are displayed in the merge image with different pseudo-colors (Fig. 6E, middle and right columns, arrowheads). In this example, we observed some initially motile MT1-MMP–mCherry vesicles moving along the neurites that became stabilized at the bead–neurite contact at both 34 s and 108 s after photobleaching. Kymograph analyses further indicated that multiple events of local capturing of MT1-MMP–mCherry vesicles were identified at agrin–bead contact sites (Fig. 6F, arrows). Nevertheless, we also observed bidirectional transport of some MT1-MMP–mCherry vesicles passing through the bead–neurite contacts without stopping. By counting the number of MT1-MMP–mCherry vesicles passing through the bead–neurite contact sites during a period of 100 s after photobleaching, we identified that 21 out of 40 (52.5%) discrete MT1-MMP–mCherry vesicles were stalled at the bead contact. These data indicate that some dynamic MT1-MMP vesicles can be locally captured at the sites induced by agrin beads.

To demonstrate that the locally captured MT1-MMP vesicles can subsequently be inserted into the membrane at the sites of agrin stimulation, we used a construct encoding MT1-MMP tagged with pHluorin, a pH-sensitive GFP variant. The sensitivity of MT1-MMP–pHluorin for detecting its surface expression in *Xenopus* primary cultures has been validated by previous experiments where there was a sequential change of culture media to those with different pHs (Chan et al., 2020a). Compared with MT1-MMP–mCherry or MT1-MMP immunostaining signals, which reveal both surface and vesicular pools of MT1-MMP proteins, we observed discrete MT1-MMP–pHluorin signals preferentially at the bead–neurite contacts (Fig. 6G), indicating agrin beads locally induce surface localization of MT1-MMP. Next, we performed photobleaching experiments on one of the bead–neurite contacts, followed by live-cell imaging to monitor the recovery of MT1-MMP–pHluorin signals at the photobleached region (Fig. 6H). In this example, we observed discrete MT1-MMP–pHluorin signals appearing at the edge of bead–neurite contact at between 8 s and 11 s after photobleaching, followed by the disappearance of the localized signals. Taken together, our findings suggested that localized agrin stimulation directs the vesicular trafficking and surface insertion of MT1-MMP proteins, which are then incorporated into the existing MT1-MMP clusters induced by agrin beads.

MT1-MMP-mediated proteolytic cleavage of neuronal Lrp4 is required for agrin-induced presynaptic differentiation

MMPs have recently been found to play a critical role in presynaptic differentiation through the proteolytic cleavage of the transmembrane Lrp4 proteins into the diffusible ectodomain fragment of Lrp4 (ecto-Lrp4) (Wu et al., 2012). The released ecto-Lrp4 then acts as a co-receptor of agrin to stimulate AChR clustering in skeletal muscles. However, whether MT1-MMP proteolytically cleaves Lrp4 to generate ecto-Lrp4 in presynaptic differentiation remains unclear. Firstly, we tested whether soluble recombinant ecto-Lrp4 could rescue the suppression of presynaptic differentiation caused by either MMP inhibition or neuronal MT1-MMP knockdown. Consistent with the data presented above, BB-94 treatment or MT1-MMP MO significantly inhibited mitochondrial and SV clustering induced by agrin beads. Interestingly, these inhibitory effects were abolished by incubating the cells with soluble recombinant ecto-Lrp4 proteins (Fig. 7). In particular, soluble ecto-Lrp4 treatment in wild-type neurons caused a slight, although not statistically significant, increase in agrin bead-induced SV and mitochondrial clustering compared to the untreated neurons (Fig. 7B). These findings suggested a requirement of MT1-MMP in agrin-Lrp4 signaling in presynaptic differentiation, and MT1-MMP-mediated proteolytic processing of endogenous neuronal Lrp4 is sufficient to produce the required amount of ecto-Lrp4 fragments for agrin-induced presynaptic differentiation.

Neuronal MT1-MMP is required for agrin-Lrp4 signaling in NMJ formation

To examine the role of MMP activity in the formation of NMJs, we used the well-established *Xenopus* nerve-muscle co-culture system

Journal of Cell Science (2020) 133, jcs246710. doi:10.1242/jcs.246710

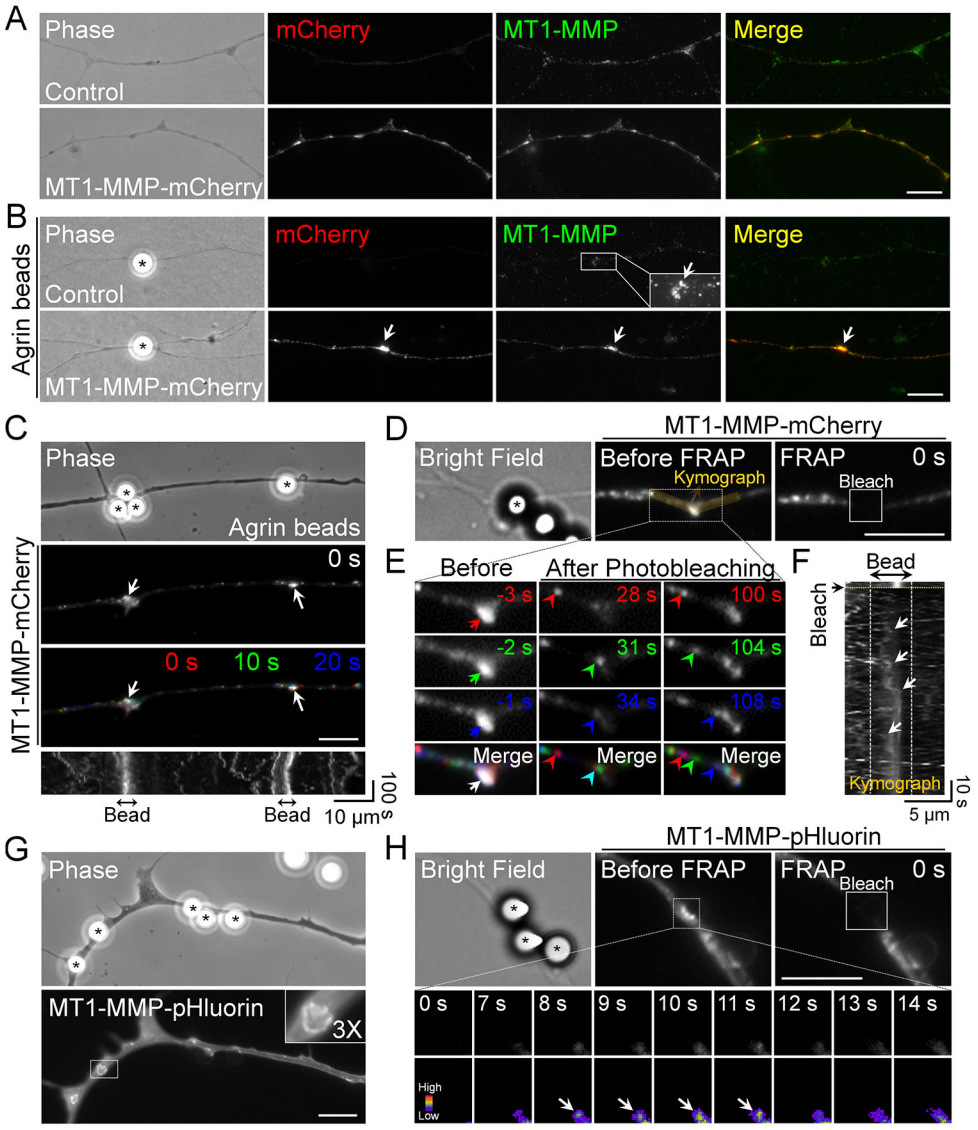

Fig. 6. Axonal trafficking and surface insertion of MT1-MMP are directed to sites of local agrin stimulation. (A) Representative images showing a similar localization pattern between endogenous MT1-MMP signals and exogenous MT1-MMP–mCherry signals in cultured neurons. (B) Representative images showing the spatial localization of endogenous MT1-MMP and exogenous MT1-MMP–mCherry signals at agrin bead–neurite contact sites. Inset shows endogenous MT1-MMP signals in the contrast-enhanced image. Asterisks indicate the bead–neurite contact sites. Arrows indicate the localization of presynaptic markers at the bead–neurite contacts. (C) Representative images showing the mobility of MT1-MMP–mCherry vesicles at bead-contact versus non-contact regions along the neurite. A pseudo-color image was constructed by merging time-lapse images from three different time points to illustrate the mobility of MT1-MMP–mCherry vesicles. Asterisks indicate the bead–neurite contact sites. Arrows indicate the immobile clusters of MT1-MMP–mCherry vesicles localized at the bead–neurite contacts. A kymograph (bottom panel) shows the stability of MT1-MMP-mCherry vesicles at the bead-contact versus non-contact regions along the neurite. (D) Representative images showing the fluorescence signals of MT1-MMP–mCherry at agrin bead–neurite contact before and after photobleaching of signals at a defined region (square). An asterisk indicates the bead–neurite contact site. (E) Time-lapse images showing MT1-MMP–mCherry signals in the dotted rectangular region (indicated in D) before and after photobleaching. Pseudo-colored merge images were constructed to indicate the position of MT1-MMP–mCherry vesicles at three different time points. Arrows indicate the immobile clusters of MT1-MMP–mCherry vesicles localized at the bead–neurite contact. Arrowheads indicate local capture of MT1-MMP–mCherry vesicles at the bead–neurite contacts. (F) A kymograph constructed from 100 frames in a 97 s time-lapse series along the yellow line (indicated in D). White arrows indicate the local capturing of multiple MT1-MMP–mCherry vesicles at the bead–neurite contacts. White dotted lines mark the boundary of an agrin bead, and a yellow dotted line indicates the time of photobleaching. (G) Representative images showing the spatial enrichment of surface MT1-MMP at agrin bead–neurite contact sites (asterisks). For clarity, the boxed region in MT1-MMP–pHluorin image was magnified and is shown in the inset. (H) Representative FRAP time-lapse images showing the spatial insertion of MT1-MMP-pHluorin induced by localized agrin stimulation, as reflected by the appearance of discrete MT1-MMP–pHluorin signals (arrows) at an agrin bead–neurite contact after photobleaching. Numbers indicate the elapsed time (in seconds) after photobleaching. For clarity, pseudo-colored images (bottom row) were included to show the relative fluorescence intensity of MT1-MMP–pHluorin. Scale bars: 10 µm with exception of kymographs, which are as indicated on the image.

to examine the effects of MMP inhibition on neuromuscular synaptogenesis. First, bath application of BB-94 significantly inhibited nerve-induced AChR clustering, a hallmark of NMJ formation, and agrin deposition along the neurites (Fig. 8A). The inhibitory effects of BB-94 on NMJ formation were demonstrated by a reduced percentage of nerve–muscle contacts with AChR clustering and agrin deposition (Fig. 8B) and a lower fluorescence intensity of these two synaptic markers at the nerve–muscle contacts

Journal of Cell Science (2020) 133, jcs246710. doi:10.1242/jcs.246710

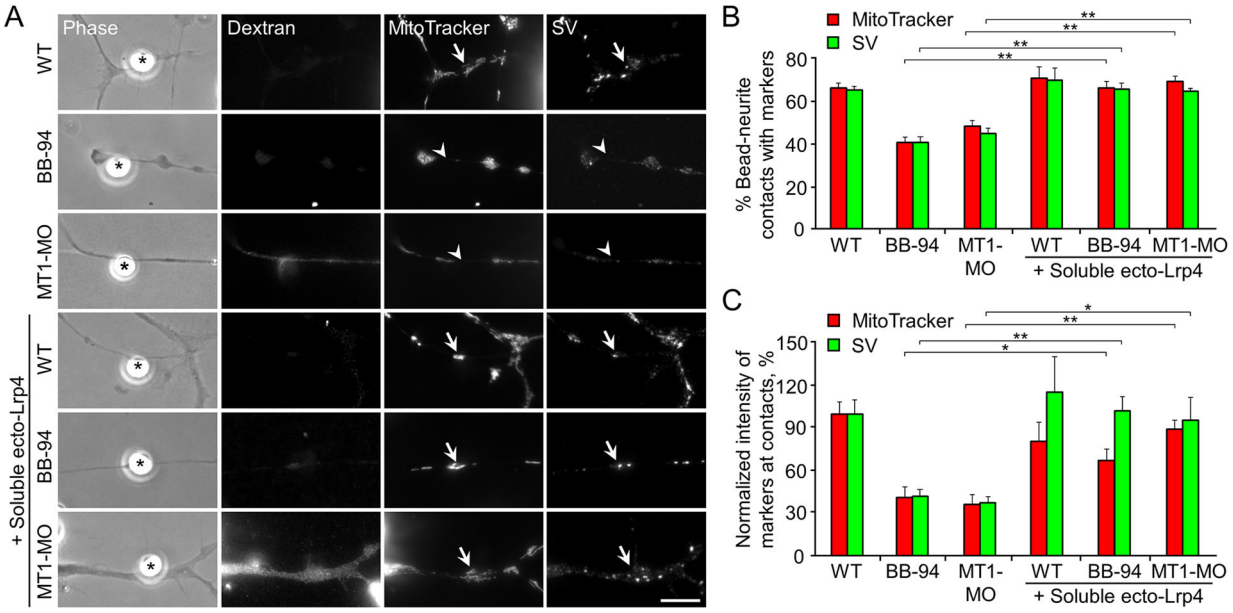

Fig. 7. Soluble ecto-Lrp4 reverses the inhibitory effect of MMP inhibition or MT1-MMP knockdown on agrin-induced presynaptic differentiation. (A) Representative images showing that soluble recombinant ecto-Lrp4 reverses the suppression of agrin-induced mitochondrial and SV clustering induced by BB-94 treatment or by MO-mediated knockdown of endogenous MT1-MMP expression (MT1-MO). Asterisks indicate the bead–neurite contact sites. Arrows and arrowheads indicate the presence and absence of presynaptic marker localization at the bead–neurite contact, respectively. (B) Quantitative analysis showing the percentage of agrin bead–neurite contacts with presynaptic markers in BB-94-treated or MT1-MO-mediated knockdown neurons with or without soluble ecto-Lrp4 treatment. *n*=150 bead–neurite contacts in each experimental group from three independent experiments. (C) Quantitative analysis showing the fluorescence intensities of agrin-induced mitochondrial and SV clusters in BB-94-treated or MT1-MO-mediated knockdown neurons with or without soluble ecto-Lrp4 treatment. *n*=90 (WT), 103 (BB-94), 99 (MT1-MO), 107 (WT+ecto-Lrp4), 128 (BB-94+ecto-Lrp4), or 93 (MT1-MO+ecto-Lrp4) bead–neurite contacts from three independent experiments. Data are mean±s.e.m. **P*<0.05; ***P*<0.01 (unpaired Student's *t*-test). Scale bar: 10 µm.

(Fig. 8C). As MT1-MMP is expressed in both motor neurons and muscle fibers, we next examined the functional roles of neuronal MT1-MMP in the formation of NMJs using chimeric nerve–muscle co-cultures consisting of MT1-MMP MO neurons and wild-type muscle cells (Fig. 8D). In wild-type co-cultures and the chimeric co-cultures containing control MO neurons, AChR clusters were prominently detected at nerve–muscle contact sites, and agrin deposition was found along the neurites. However, in the chimeric co-cultures containing MT1-MMP MO neurons, both nerve-induced AChR clustering and agrin deposition along the neurites were significantly suppressed (Fig. 8D–F). To examine the requirement of neuronal MT1-MMP for NMJ development *in vivo*, we next performed microinjection of MT1-MMP MO, together with fluorescent dextran as a cell lineage tracer, into a specific blastomere of stage 6 (32-cell) embryos (Fig. 8G), which later predominantly give rise to the spinal cord tissues as determined by the well-defined fate map of *Xenopus laevis* (Moody, 1987). We found that knockdown of neuronal MT1-MMP affected the synaptic structures of developing *Xenopus* NMJs *in vivo*, as evidenced by the reduction of both presynaptic SV2 and postsynaptic AChR clusters compared with that seen in the wild-type embryos (Fig. 8H).

Consistent with our previous study using whole-body MT1-MMP-knockout mice (Chan et al., 2020a), here we also found that knockdown of MT1-MMP preferentially in spinal cord tissues caused a reduced axonal length in motor neurons at stage 32 *Xenopus* embryos *in vivo* (Fig. 8H, arrows). The essential requirement of MT1-MMP for neuronal outgrowth was further validated by examining MT1-MMP MO cultured neurons, which showed a significant reduction in neurite outgrowth and increased percentage of neurites with collapsed growth cones (Fig. S7). Collectively, this study indicates that neuronal MT1-MMP is an important regulator of axonal growth and neuromuscular synaptogenesis *in vitro* and *in vivo*.

DISCUSSION

In this study, we first reported an intrinsic regulation in the transition of *Xenopus* spinal neurons from the outgrowth to the synaptogenic phase *in vitro*, in which neuronal MT1-MMP regulates presynaptic differentiation by means of mediating ECM degradation to allow agrin deposition, as well as by producing soluble ecto-Lrp4 proteolytically to modulate agrin signaling (Fig. 8I). Although dissociated neural tube tissues of *Xenopus* embryos contain different neuronal types, previous electrophysiological studies have shown that more than 60% of the neuronal population in cultured *Xenopus* spinal neurons release acetylcholine upon their direct muscle contact (Chow and Poo, 1985). Importantly, imaging studies further demonstrated that AChR clustering could be detected at up to 90% nerve–muscle contacts (Peng et al., 2003). These studies therefore indicate that the major neuronal type in *Xenopus* spinal neuronal cultures is indeed motor neurons.

Young cultured *Xenopus* spinal neurons underwent robust axonal outgrowth as demonstrated by the presence of large fan-shaped growth cone structures that are composed of actin-based dynamic filopodial and lamellipodial protrusions (Dent et al., 2011; Gomez and Letourneau, 2014). The direction in which the growth cone moves greatly relies on its interaction with the extracellular environment. As the neuron matures, it degrades the surrounding ECM molecules to allow the deposition of nerve-derived agrin, which is one of the most crucial synaptogenic factors in NMJ development. Here, we showed that this transition from outgrowth-to-synaptogenesis phase in young neuronal cultures was greatly accelerated upon treatment with exogenous recombinant agrin.

Journal of Cell Science (2020) 133, jcs246710. doi:10.1242/jcs.246710

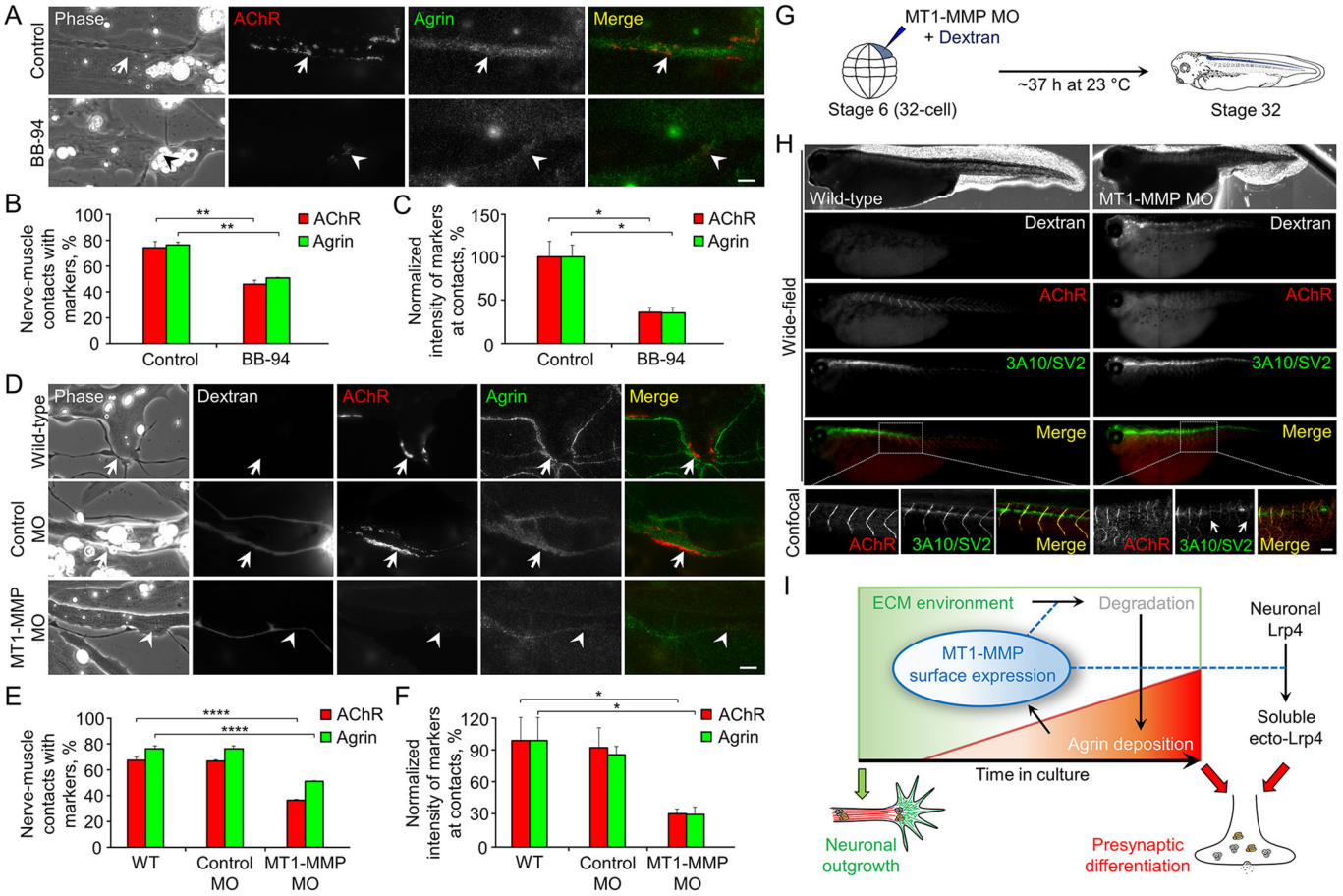

Fig. 8. Neuronal MT1-MMP is required for NMJ formation *in vitro* and *in vivo*. (A) Representative images showing that BB-94 suppresses agrin deposition and nerve-induced AChR clustering. Arrows indicate the localization of agrin deposition and AChR clusters at the nerve–muscle contacts. Arrowheads indicate the reduced signals of both agrin deposition and AChR clusters at the nerve–muscle contacts. (B) Quantitative analysis showing that BB-94 treatment inhibits agrin deposition and nerve-induced AChR clustering at the nerve–muscle contact. *n*=150 nerve-muscle contacts in each experimental group from three independent experiments. (C) Quantitative analysis showing that BB-94 treatment reduces the fluorescence intensity of AChR and agrin deposition at the nerve–muscle contact. *n*=30 nerve–muscle contacts in each experimental group from three independent experiments. (D) Representative images showing that neuronal MT1-MMP knockdown inhibits agrin deposition and nerve-induced AChR clustering at the nerve–muscle contact. Fluorescent dextran indicates the presence of MO in neurons, but not in muscle cells. Arrows indicate the localization of agrin deposition and AChR clusters at the nerve–muscle contacts. Arrowheads indicate the reduced signals of both agrin deposition and AChR clusters at the nerve–muscle contacts. (E) Quantitative analysis showing that neuronal MT1-MMP knockdown inhibits agrin deposition and nerve-induced AChR clustering at the nerve–muscle contact. *n*=150 nerve–muscle contacts in each experimental group from three independent experiments. (F) Quantitative analysis showing that neuronal MT1-MMP knockdown reduces fluorescence intensity of AChR and agrin deposition at the nerve–muscle contact. *n*=30 nerve–muscle contacts in each experimental group from three independent experiments. (G) Schematic diagram showing the specific blastomere selected for microinjection of MT1-MMP MO and fluorescent dextran in stage 6 *Xenopus* embryos. The microinjected blastomere will subsequently develop to spinal cord tissues primarily at stage 32 embryos. (H) Representative wide-field and confocal images showing that neuronal MT1-MMP knockdown preferentially in spinal cord tissues affects presynaptic and postsynaptic structures at *Xenopus* NMJs *in vivo*. Arrows indicate the axonal growth defects in neuronal MT1-MMP knockdown embryos. (I) Working model suggesting dual functional roles of MT1-MMP activity in agrin-induced presynaptic differentiation via regulating agrin deposition and signaling through ECM degradation and Lrp4 activation, respectively. Blue dotted lines represent MT1-MMP proteolytic activity. Data are mean±s.e.m. **P*<0.05; ***P*<0.01; *****P*<0.0001 [unpaired Student's *t*-test (B,C), one-way ANOVA with Dunnett's multiple comparison test (E,F)]. Scale bars: 10 µm (A,D); 100 µm (H).

Specifically, agrin treatment of young neurons caused a significant increase in the presence of two of the well-defined presynaptic markers, SVs and mitochondrial clustering (Dai and Peng, 1995; Lee and Peng, 2006, 2008), along the neurites to a comparable extent to that observed in the older untreated neurons. In addition, agrin-induced acceleration of synaptogenic transition in young neurons was further reflected by a reduction of neurite extension and an increase in collapsed growth cones. Interestingly, exogenous agrin treatment did not cause any significant effects on the older neurons, indicating that the developmentally regulated secretion and deposition of endogenous agrin serve as an intrinsic molecular switch for the transition from outgrowth to synaptogenic phase of cultured spinal neurons. It is noteworthy that *Xenopus* spinal neurons can survive up to 5 days in culture, in the absence of tropic factor supplementation (Peng et al., 2003). In addition, it is true that motor axons keep growing until they make synapses in an *in vivo* environment. As explained by the classical neurotrophic hypothesis (Davies, 1988; Henderson, 1996), target cells secrete various neurotrophic factors that act to promote the survival, outgrowth, and/or pathfinding of neurons. In agreement with other previous studies using ciliary ganglion neurons (Campagna et al., 1997) and hippocampal neurons (Böse et al., 2000), our findings further demonstrate that agrin serves as a differentiation-inducing stop signal for cultured spinal neurons. Importantly, our present study

Journal of Cell Science (2020) 133, jcs246710. doi:10.1242/jcs.246710

suggests that the spatiotemporal control of agrin deposition, through modulating the surrounding ubiquitously expressed ECM proteins, is a novel intrinsic neuronal property underlying the transition from axonal outgrowth to synaptogenesis, which is difficult to study in the complex *in vivo* environment.

It has been suggested that ECM degradation mediated by MMP activity plays a permissive role in axonal extension by allowing growth cone advance and pathfinding across the surrounding tissues (Miller et al., 2008; Short et al., 2016). Within the central domain of growth cones, actin-rich basal membrane protrusions, termed invadosomes, facilitate the targeting of MMPs to mediate local ECM remodeling through their proteolytic activities (Santiago-Medina et al., 2015). In this study, we demonstrated that either global inhibition of multiple MMPs, by BB-94 treatment, or reduced expression of a specific MMP, by MT1-MMP MO, suppressed agrin-induced presynaptic differentiation in neurons and nerve-induced AChR clustering at NMJs. Photobleaching experiments in cultured spinal neurons overexpressing MT1-MMP–mCherry demonstrated that MT1-MMP vesicles were bidirectionally transported along the neurites, and some of the locally captured MT1-MMP vesicles were inserted at the agrin bead–neurite contact sites. In migrating keratinocytes, the vesicular trafficking and surface insertion of MT1-MMP are targeted to the sites of focal adhesion via cytoplasmic linker-associated protein-mediated microtubule capture (Stehbens et al., 2014). It is suggested that growth cones employ similar cellular and molecular machineries as other migrating cells to 'clutch' retrograde actin flow in the surrounding ECM environment (Short et al., 2016), possibly through site-directed trafficking and surface targeting of MT1-MMP. Our recent study demonstrated that MT1-MMP-knockout mice exhibit an obvious presynaptic defect in phrenic nerves, which are innervating diaphragm muscles, at embryonic stages (Chan et al., 2020a), suggesting the requirement of MT1-MMP-mediated ECM modulation in neuronal outgrowth and presynaptic differentiation (Chan et al., 2020b). Consistent with this observation, we here also report that both pharmacological inhibition of MMP activity and molecular manipulation of endogenous MT1-MMP expression greatly induced growth cone collapse, leading to a significant reduction in neurite outgrowth of cultured *Xenopus* spinal neurons. By knocking down MT1-MMP preferentially in spinal cord tissues, we observed structural defects in presynaptic and postsynaptic structures in *Xenopus* embryos, suggesting that neuronal MT1-MMP is essential for NMJ development *in vivo*. Nevertheless, this warrants further investigations and validations using tissue-specific MT1-MMP-knockout animal models in future studies.

Previous studies have suggested that MMP-3 and other MMPs are involved in the removal of agrin from synaptic basal lamina at adult NMJs (Patel et al., 2012; VanSaun et al., 2003). At developing NMJs, however, our recent study demonstrated that the pattern and intensity of cell-free endogenous agrin tracks cultured with muscle cells were largely unaffected by MMP inhibitors (Chan et al., 2020a). Therefore, we hypothesize that the spatiotemporal control of MT1-MMP intracellular trafficking and surface localization focally regulate degradation and remodeling of different ubiquitously expressed ECM proteins, in order to clear the surrounding extracellular environment for the subsequent deposition of synapse-specific proteins (e.g. the synaptogenic factors agrin and neuregulin, and the synapse-specific ECM proteins laminin β2 and collagen IV). Consistent with this notion, we also found that the synapse-specific protein agrin is resistant to MMP-mediated degradation in this study. Taken together, these data rule out the possibility that agrin is a proteolytic target of either muscle or neuronal MT1-MMP activity.

Local presentation of some heparan sulfate proteoglycan (HSPG)-bound growth factors (e.g. bFGF and heparin-binding growth-associated molecule) via polystyrene beads can effectively induce both cytoplasmic and membranous presynaptic specializations at the bead–neurite contact sites in a spatiotemporally controllable manner (Dai and Peng, 1995; Rauvala and Peng, 1997). Here, we found that polystyrene beads coated with the C-terminal fragment of recombinant agrin proteins locally induce presynaptic differentiation to an extent similar to bFGF-coated beads. This recombinant agrin fragment contains the amino acid sequence from Ala1153 to Pro1959, with a highly conserved nine amino acid insert at the Z site, which is known as one of the neural agrin isoforms produced selectively by motor neurons for inducing acetylcholine receptor clustering in muscle cells (Ferns et al., 1992; Gesemann et al., 1995; Ruegg et al., 1992). On the postsynaptic side, agrin-coated beads effectively induce local AChR clustering in cultured *Xenopus* muscle cells (Lee et al., 2009), further suggesting that agrin-Lrp4 signaling is a shared synaptogenic pathway that regulates both presynaptic and postsynaptic differentiation at developing NMJs.

In postsynaptic differentiation, the role of the agrin-Lrp4-MuSK signaling pathway has been well established (Kim et al., 2008; Zhang et al., 2008). In this study, we further demonstrated a similar molecular mechanism initiated by agrin for the induction of presynaptic differentiation at developing NMJs. Consistent with the previous studies in mouse models (Wu et al., 2012; Yumoto et al., 2012), we found that Lrp4 is endogenously expressed in both muscles and spinal neurons cultured from *Xenopus* embryos as shown by the RT-PCR results. In Lrp4-null mice, nerve processes extend across a larger area of diaphragm muscles, rather than having the arborized nerve terminals concentrated at the central region of the muscles in the wild-type animals. This indicates the crucial requirement of Lrp4 expression for both preventing aberrant axonal growth and initiating presynaptic differentiation. Interestingly, distinct functions of motoneuron and muscle Lrp4 have been proposed to make a concerted effort in regulating NMJ development *in vivo* (Wu et al., 2012). MMP-mediated extracellular cleavage of single-transmembrane Lrp4 proteins is believed to generate soluble ecto-Lrp4, which in turn acts as a co-receptor of agrin to induce AChR clustering. To further determine the source of Lrp4 for NMJ development, we found that ecto-Lrp4 treatment can rescue the inhibitory effects on presynaptic and postsynaptic differentiation caused by Lrp4 knockdown in either spinal neurons or muscles (Fig. S8). However, a previous study showed that Lrp4 in motor neurons is dispensable for NMJ formation, as evidenced by the normal NMJ structures in P0 diaphragm muscles of motor neuron-specific Lrp4-deficient mice (Wu et al., 2012). These data suggest that while MT1-MMP-mediated proteolytic activation of Lrp4 from both spinal neurons and muscle cells is required for early NMJ development (E13.5–E18.5), ecto-Lrp4 generated by muscle Lrp4 is sufficient to induce and maintain normal NMJ development in neuronal Lrp4-deficient animals at later stages. In the central nervous system, recent studies have also demonstrated that presynaptic Lrp4 promotes dendritic development and synapse formation in mouse hippocampal and cortical neurons (Karakatsani et al., 2017) and synaptogenesis of excitatory neurons in *Drosophila* (Mosca et al., 2017). Therefore, the results of this study suggest that the MT1-MMP activity has a role for generating ecto-Lrp4 in the regulation of synapse formation and plasticity in both central and peripheral nervous systems of different species.

Journal of Cell Science (2020) 133, jcs246710. doi:10.1242/jcs.246710

MATERIALS AND METHODS

Xenopus embryo microinjection and primary cell culture

All experiments involving *Xenopus* frogs and embryos were carried out in accordance with the approved protocols by the Committee on the Use of Live Animals in Teaching and Research (CULATR) of The University of Hong Kong. DNA constructs encoding mCherry- or pHluorin-tagged MT1-MMP (a gift from Cheng-Han Yu, The University of Hong Kong) were microinjected into the one- or two-cell stage *Xenopus* embryos using an oocyte injector Nanoject (Drummond Scientific) as previously described (Lee et al., 2009, 2014). To knock down the endogenous expression of specific proteins, custom-designed antisense MO sequences (agrin: 5′-CTACTGCTGCTCAAAGGAAAACCTA-3′; Lrp4: 5′-CCATAATGC-CACTTCTCCCCCTG-3′; MT1-MMP: 5′-CCAGGCTGCTCTCAGAGG-CTCCATC-3′; Gene Tools) were used. The control MO sequence (5′-CCTCTTACCTCAGTTACAATTTATA-3′; Gene Tools) was used as a negative control. Alexa Fluor 488- or tetramethylrhodamine-conjugated dextran (Thermo Fisher Scientific) was co-injected into the embryos as a fluorescent cell lineage tracer.

Wild-type or microinjected embryos were dissected when they reached Nieuwkoop and Faber stage 19–22. Neural tubes and/or myotomes were collected after collagenase treatment and then dissociated in Ca^{2+}/Mg^{2+}-free solution as previously described (Peng et al., 1991). The dissociated cells were plated on acid-washed glass coverslips coated with entactin-collagen IV-laminin (71.4 µg/ml; Merck Millipore). For fluorescent gelatin coating, the acid-washed glass coverslips were coated with Oregon Green- or FITC-conjugated gelatin (1 mg/ml; Thermo Fisher Scientific) according to an established protocol (Díaz, 2013).

All chemicals were purchased from Sigma unless otherwise specified. Cell cultures were maintained in culture medium containing 10% Leibovitz's L-15 medium (v/v), 87% Steinberg's solution (v/v; 60 mM NaCl, 0.67 mM KCl, 0.35 mM $Ca(NO_3)_2$, 0.83 mM $MgSO_4$, 10 mM HEPES pH 7.4), 1% fetal bovine serum (v/v; Thermo Fisher Scientific), 1% penicillin/streptomycin (v/v; Thermo Fisher Scientific) and 1% gentamicin sulfate (v/v; Thermo Fisher Scientific). The cultured neurons were kept at room temperature for different durations as specified prior to the experiments. For the nerve–muscle co-cultures, dissociated spinal neurons were plated on 2-day-old muscle cultures to induce synaptogenesis. In some experimental groups, the following reagents were added to the culture medium 1 h before plating the neurons: recombinant rat agrin (R&D Systems), recombinant Lrp4 (R&D Systems) or BB-94 (ApexBio). To locally induce presynaptic differentiation in cultured neurons, 4.5 µm polystyrene beads (Polysciences) were coated with 100 µg/ml recombinant human bFGF (ProSpec) or rat agrin based on the procedures previously described (Dai and Peng, 1995; Lee et al., 2009), while the beads coated with 100 µg/ml bovine serum albumin (BSA, Sigma) served as a negative control.

Live-cell staining

To label mitochondria, live cultured neurons were stained with MitoTracker® Red CMXRos (50 nM; Thermo Fisher Scientific) for 5 min and then rinsed with culture medium three times before mounting the coverslip for imaging. To label the readily releasable pool of SV clusters, the cultured neurons were stained with FM 1-43 fixable dye (Thermo Fisher Scientific) in a high potassium solution (30 mM NaCl, 51 mM KCl, 2 mM $CaCl_2$, 5 mM HEPES pH 7.4) for 5 min, and then rinsed with culture medium three times prior to imaging. FM1-43 unloading was then performed by treating the live neurons with the high potassium solution for 15 min. Agrin deposition was visualized by labeling with anti-agrin monoclonal antibody [1:100; cat. # 6D2-s, Developmental Studies Hybridoma Bank (DSHB)], followed by Alexa Fluor 488-, 546-, or 647-conjugated secondary antibodies (1:400; Thermo Fisher Scientific). To label synaptic AChR clusters, nerve–muscle co-cultures were stained with 1 µg/ml Alexa Fluor 488- or 546-conjugated α-bungarotoxin (α-BTX, Thermo Fisher Scientific) for 45 min, followed by extensive washing with the culture medium for at least 3 times.

Cell fixation and immunostaining

Coverslips were fixed with 4% paraformaldehyde (Sigma) for 15 min, followed by cell permeabilization with 0.1% Triton X-100 (Sigma) for 10 min. For labeling transmembrane or secreted proteins, the cell permeabilization step was skipped. Cells were then blocked in 2% BSA at 4°C overnight. The fixed cultures were labeled with primary antibodies, including anti-synaptotagmin 1 (1:200; cat. # mab 48; Developmental Studies Hybridoma Bank), anti-synapsin 1 (1:1000; cat. # A6442; Thermo Fisher Scientific), anti-phosphotyrosine (1:100; cat. # 05-321; Millipore), anti-MT1-MMP (1:100; cat. # MAB3328; Millipore), or anti-Lrp4 (1:200; cat. # A10172; ABclonal Technology), for 2 h, followed by Alexa Fluor 488, 546 or 647 secondary antibodies (1:400; Thermo Fisher Scientific) for 45 min. Coverslips were then mounted on glass slides with the anti-bleaching reagent fluoromount-G (cat. # 00-4958-02; Thermo Fisher Scientific) for later observation.

Total RNA extraction and RT-PCR

Total RNA from 1-day-old muscle, spinal neuron or nerve–muscle cultures were extracted with RNAiso Plus (Takara), followed by incubation with isopropanol and glycogen at −20°C overnight and washed with 70% ethanol prior to its resuspension in DNase and RNase-free water (Thermo Fisher Scientific). The total RNAs were reverse transcribed by using a high-capacity cDNA reverse transcription kit (Thermo Fisher Scientific). PCR primers for *Xenopus* Lrp4 were designed based on the NCBI sequence XM_018257331.1, forward, 5′-GACATGTAAGAGCTTGCGGG-3′, and reverse, 5′-AATGAGCAAGACGGGGAAGA-3′. PCR primers for *Xenopus* motor neuron and pancreas homeobox 1 (mnx1) were designed based on the NCBI sequence NM_001096823.1, forward, 5′-CCCTACTCCCAGATGCAGAG-3′, and reverse, 5′-TGACTGGTAA-ACGCTGTCCT-3′. PCR primers for *Xenopus* myogenic differentiation 1 (myoD1) were designed based on the NCBI sequence NM_001087823.1, forward: 5′-ACCAGAGACTCCCCAAAGTG-3′, and reverse, 5′-GGGG-CTGTCAGTGTAGAAGT-3′. PCR primers for *Xenopus* agrin were designed based on the NCBI sequence XM_018227826.1, forward, 5′-T-CTCTGGAGGACAATGTGAGAAAGC-3′, and reverse, 5′-CCTGAGT-GGCTTCAGTCTTTATGC-3′. PCR primers for *Xenopus* GAPDH were designed based on the NCBI sequence NM_001087098.1, forward, 5′-G-TGTATGTGGTGGAATCT-3′, and reverse, 5′-AAGTTGTCGTTGATG-ACCTTTGC-3′. PCR was performed using Phusion II High Fidelity DNA polymerase (Thermo Fisher Scientific) on Takara PCR Thermal Cycler Dice. PCR products were loaded on 1.5% agarose gel and separated by gel electrophoresis, followed by the visualization using ultraviolet transilluminator.

Immunocytochemistry of whole-mount *Xenopus* embryos

To knockdown the endogenous expression of MT1-MMP preferentially in spinal cord, MT1-MMP MO or control MO was co-injected with Alexa Fluor 488-conjugated dextran (Thermo Fisher Scientific) into a specific blastomere of 32-cell stage *Xenopus* embryos, as determined by the well-established fate map (Moody, 1987). After reaching Nieuwkoop and Faber stage 32, wild-type and microinjected embryos were fixed in 4% PFA for 1 h at room temperature, followed with permeabilization with 1% Triton X-100. The embryos were blocked in 10% fetal bovine serum at 4°C overnight. The embryos were then incubated with primary antibodies against neurofilament 3A10 (1:50; cat. # 3A10-s, DSHB) and synaptic vesicle marker SV2 (1:50; cat. # SV2-s, DSHB) at 4°C overnight. After extensive washing, the embryos were stained with Alexa Fluor 647-conjugated anti-mouse-IgG secondary antibody (1:200; Thermo Fisher Scientific) and Alexa Fluor 546-conjugated α-BTX (1:500; Thermo Fisher Scientific). After extensive washing with PBS with 1% Triton X-100, the embryos were mounted on glass slides with Fluoromount-G mounting medium (Thermo Fisher Scientific).

Fluorescence recovery after photobleaching

FRAP was performed by using Nikon total internal reflection fluorescence (TIRF) microscope. The region of agrin bead–neurite contact site in MT1-MMP–mCherry- or MT1-MMP–pHluorin-expressing neurons was selected for photobleaching. 11 images at 0.2 s interval were taken before the photobleaching to obtain a baseline fluorescence intensity, then 150 images (MT1-MMP–mCherry) or 200 images (MT1-MMP–pHluorin) at 1 s interval were taken afterwards to visualize the vesicular trafficking and fluorescence recovery of MT1-MMP–mCherry or MT1-MMP–pHluorin

signals at the photobleached area. Kymographs were constructed in ImageJ using the selected frames from the time-lapse series.

Microscopy and data analysis

Fluorescence imaging on live or fixed cells was performed on an inverted wide-field fluorescence microscope (IX-83, Olympus) using PlanApo 60× NA 1.42 phase-contrast oil immersion objective lens. The microscope was controlled through imaging software Micro-Manager (Open Imaging) and images were taken by ORCA-Flash 4.0 LT+ digital CMOS camera (Hamamatsu). For whole-mount *Xenopus* embryo imaging, *z*-stack images were acquired on confocal microscope (LSM880, Carl Zeiss) controlled by the imaging software ZEN (Carl Zeiss) using a 10× NA 0.45 phase-contrast objective lens.

All images were acquired with identical parameters between control and experimental groups. The percentage values were quantified by scoring 150 samples from at least three independent experiments. For quantifying the fluorescence intensities, at least 30 samples from at least three independent experiments were collected and analyzed. Data analyses were conducted using ImageJ (NIH), and the statistical analyses were performed using Prism 7 (GraphPad).

Acknowledgements

We thank Zora Chan for her assistance in some confocal imaging experiments, and the Imaging Core Facility at HKU Medicine for image acquisition and analysis.

Competing interests

The authors declare no competing or financial interests.

Author contributions

Conceptualization: C.W.L.; Methodology: M.J.O., C.W.L.; Validation: M.J.O., A.C.-K.T., C.W.L.; Formal analysis: M.J.O., C.W.L.; Investigation: M.J.O., A.C.-K.T., C.W.L.; Resources: C.W.L.; Data curation: M.J.O., C.W.L.; Writing - original draft: C.W.L.; Writing - review & editing: M.J.O., A.C.-K.T., C.W.L.; Visualization: M.J.O., C.W.L.; Supervision: C.W.L.; Project administration: C.W.L.; Funding acquisition: C.W.L.

Funding

This project was partly supported by the Early Career Grant (27102316) and General Research Fund (17100718 and 17100219) from Research Grants Council of Hong Kong, the Health and Medical Research Fund (04151086) from Food and Health Bureau of Hong Kong, and the Seed Fund Programme for Basic Research from The University of Hong Kong (201811159078 and 201910159151) to C.W.L. The funders had no role in study design, data collection and interpretation, or the decision to submit the work for publication.

Supplementary information

Supplementary information available online at
https://jcs.biologists.org/lookup/doi/10.1242/jcs.246710.supplemental

Peer review history

The peer review history is available online at
https://jcs.biologists.org/lookup/doi/10.1242/jcs.246710.reviewer-comments.pdf

References

Bezakova, G., Helm, J. P., Francolini, M. and Lømo, T. (2001). Effects of purified recombinant neural and muscle agrin on skeletal muscle fibers in vivo. *J. Cell Biol.* **153**, 1441-1452. doi:10.1083/jcb.153.7.1441

Böse, C. M., Qiu, D., Bergamaschi, A., Gravante, B., Bossi, M., Villa, A., Rupp, F. and Malgaroli, A. (2000). Agrin controls synaptic differentiation in hippocampal neurons. *J. Neurosci.* **20**, 9086-9095. doi:10.1523/JNEUROSCI.20-24-09086.2000

Campagna, J. A., Ruegg, M. A. and Bixby, J. L. (1997). Evidence that agrin directly influences presynaptic differentiation at neuromuscular junctions in vitro. *Eur. J. Neurosci.* **9**, 2269-2283. doi:10.1111/j.1460-9568.1997.tb01645.x

Chan, Z. C.-K., Kwan, H.-L. R., Wong, Y. S., Jiang, Z., Zhou, Z., Tam, K. W., Chan, Y.-S., Chan, C. B. and Lee, C. W. (2020a). Site-directed MT1-MMP trafficking and surface insertion regulate AChR clustering and remodeling at developing NMJs. *eLife* **9**, e54379. doi:10.7554/elife.54379

Chan, Z. C.-K., Oentaryo, M. J. and Lee, C. W. (2020b). MMP-mediated modulation of ECM environment during axonal growth and NMJ development. *Neurosci. Lett.* **724**, 134822. doi:10.1016/j.neulet.2020.134822

Chow, I. and Poo, M. M. (1985). Release of acetylcholine from embryonic neurons upon contact with muscle cell. *J. Neurosci.* **5**, 1076-1082. doi:10.1523/JNEUROSCI.05-04-01076.1985

Dai, Z. and Peng, H. B. (1995). Presynaptic differentiation induced in cultured neurons by local application of basic fibroblast growth factor. *J. Neurosci.* **15**, 5466-5475. doi:10.1523/JNEUROSCI.15-08-05466.1995

Dai, Z. and Peng, B.H. (1996). From neurite to nerve terminal: induction of presynaptic differentiation by target-derived signals. *Semin. Neurosci.* **8**, 97-106. doi:10.1006/smns.1996.0013

Dai, Z. and Peng, H. B. (1998). Fluorescence microscopy of calcium and synaptic vesicle dynamics during synapse formation in tissue culture. *Histochem. J.* **30**, 189-196. doi:10.1023/A:1003247403685

Davies, A. M. (1988). The emerging generality of the neurotrophic hypothesis. *Trends Neurosci.* **11**, 243-244. doi:10.1016/0166-2236(88)90099-9

Dent, E. W., Gupton, S. L. and Gertler, F. B. (2011). The growth cone cytoskeleton in axon outgrowth and guidance. *Cold Spring Harb. Perspect. Biol.* **3**, a001800. doi:10.1101/cshperspect.a001800

Deryugina, E. I., Ratnikov, B., Monosov, E., Postnova, T. I., DiScipio, R., Smith, J. W. and Strongin, A. Y. (2001). MT1-MMP initiates activation of pro-MMP-2 and integrin alphavbeta3 promotes maturation of MMP-2 in breast carcinoma cells. *Exp. Cell Res.* **263**, 209-223. doi:10.1006/excr.2000.5118

Díaz, B. (2013). Invadopodia detection and gelatin degradation assay. *Bio Protoc.* **3**, e997. doi:10.21769/bioprotoc.997

Ferns, M., Hoch, W., Campanelli, J. T., Rupp, F., Hall, Z. W. and Scheller, R. H. (1992). RNA splicing regulates agrin-mediated acetylcholine receptor clustering activity on cultured myotubes. *Neuron* **8**, 1079-1086. doi:10.1016/0896-6273(92)90129-2

Gesemann, M., Denzer, A. J. and Ruegg, M. A. (1995). Acetylcholine receptor-aggregating activity of agrin isoforms and mapping of the active site. *J. Cell Biol.* **128**, 625-636. doi:10.1083/jcb.128.4.625

Gomez, T. M. and Letourneau, P. C. (2014). Actin dynamics in growth cone motility and navigation. *J. Neurochem.* **129**, 221-234. doi:10.1111/jnc.12506

Greengard, P., Browning, M. D., McGuinness, T. L. and Llinas, R. (1987). Synapsin I, a phosphoprotein associated with synaptic vesicles: possible role in regulation of neurotransmitter release. *Adv. Exp. Med. Biol.* **221**, 135-153. doi:10.1007/978-1-4684-7618-7_11

Henderson, C. E. (1996). Role of neurotrophic factors in neuronal development. *Curr. Opin. Neurobiol.* **6**, 64-70. doi:10.1016/S0959-4388(96)80010-9

Itoh, Y. (2015). Membrane-type matrix metalloproteinases: their functions and regulations. *Matrix Biol.* **44-46**, 207-223. doi:10.1016/j.matbio.2015.03.004

Karakatsani, A., Marichal, N., Urban, S., Kalamakis, G., Ghanem, A., Schick, A., Zhang, Y., Conzelmann, K.-K., Rüegg, M. A., Berninger, B. et al. (2017). Neuronal LRP4 regulates synapse formation in the developing CNS. *Development* **144**, 4604-4615. doi:10.1242/dev.150110

Kerstein, P. C., Nichol, R. I., IV and Gomez, T. M. (2015). Mechanochemical regulation of growth cone motility. *Front. Cell. Neurosci.* **9**, 244. doi:10.3389/fncel.2015.00244

Kim, N., Stiegler, A. L., Cameron, T. O., Hallock, P. T., Gomez, A. M., Huang, J. H., Hubbard, S. R., Dustin, M. L. and Burden, S. J. (2008). Lrp4 is a receptor for Agrin and forms a complex with MuSK. *Cell* **135**, 334-342. doi:10.1016/j.cell.2008.10.002

Lee, C. W. and Peng, H. B. (2006). Mitochondrial clustering at the vertebrate neuromuscular junction during presynaptic differentiation. *J. Neurobiol.* **66**, 522-536. doi:10.1002/neu.20245

Lee, C. W. and Peng, H. B. (2008). The function of mitochondria in presynaptic development at the neuromuscular junction. *Mol. Biol. Cell* **19**, 150-158. doi:10.1091/mbc.e07-05-0515

Lee, C. W., Han, J., Bamburg, J. R., Han, L., Lynn, R. and Zheng, J. Q. (2009). Regulation of acetylcholine receptor clustering by ADF/cofilin-directed vesicular trafficking. *Nat. Neurosci.* **12**, 848-856. doi:10.1038/nn.2322

Lee, C. W., Zhang, H., Geng, L. and Peng, H. B. (2014). Crosslinking-induced endocytosis of acetylcholine receptors by quantum dots. *PLoS ONE* **9**, e90187. doi:10.1371/journal.pone.0090187

Li, Z., Takino, T., Endo, Y. and Sato, H. (2017). Activation of MMP-9 by membrane type-1 MMP/MMP-2 axis stimulates tumor metastasis. *Cancer Sci.* **108**, 347-353. doi:10.1111/cas.13134

Li, L., Xiong, W.-C. and Mei, L. (2018). Neuromuscular junction formation, aging, and disorders. *Annu. Rev. Physiol.* **80**, 159-188. doi:10.1146/annurev-physiol-022516-034255

Lowery, L. A. and Van Vactor, D. (2009). The trip of the tip: understanding the growth cone machinery. *Nat. Rev. Mol. Cell Biol.* **10**, 332-343. doi:10.1038/nrm2679

Miller, C. M., Page-McCaw, A. and Broihier, H. T. (2008). Matrix metalloproteinases promote motor axon fasciculation in the Drosophila embryo. *Development* **135**, 95-109. doi:10.1242/dev.011072

Moody, S. A. (1987). Fates of the blastomeres of the 32-cell-stage Xenopus embryo. *Dev. Biol.* **122**, 300-319. doi:10.1016/0012-1606(87)90296-X

Mosca, T. J., Luginbuhl, D. J., Wang, I. E. and Luo, L. (2017). Presynaptic LRP4 promotes synapse number and function of excitatory CNS neurons. *eLife* **6**, e27347. doi:10.7554/elife.27347

Nagase, H., Visse, R. and Murphy, G. (2006). Structure and function of matrix metalloproteinases and TIMPs. *Cardiovasc. Res.* **69**, 562-573. doi:10.1016/j.cardiores.2005.12.002

Omotade, O. F., Pollitt, S. L. and Zheng, J. Q. (2017). Actin-based growth cone motility and guidance. *Mol. Cell. Neurosci.* **84**, 4-10. doi:10.1016/j.mcn.2017.03.001

Patel, T. R., Butler, G., McFarlane, A., Xie, I., Overall, C. M. and Stetefeld, J. (2012). Site specific cleavage mediated by MMPs regulates function of agrin. *PLoS ONE* **7**, e43669. doi:10.1371/journal.pone.0043669

Peng, H. B. (1983). Cytoskeletal organization of the presynaptic nerve terminal and the acetylcholine receptor cluster in cell cultures. *J. Cell Biol.* **97**, 489-498. doi:10.1083/jcb.97.2.489

Peng, H. B., Markey, D. R., Muhlach, W. L. and Pollack, E. D. (1987). Development of presynaptic specializations induced by basic polypeptide-coated latex beads in spinal cord cultures. *Synapse* **1**, 10-19. doi:10.1002/syn.890010104

Peng, H. B., Baker, L. P. and Chen, Q. (1991). Tissue culture of Xenopus neurons and muscle cells as a model for studying synaptic induction. *Methods Cell Biol.* **36**, 511-526. doi:10.1016/S0091-679X(08)60294-0

Peng, H. B., Yang, J.-F., Dai, Z., Lee, C. W., Hung, H. W., Feng, Z. H. and Ko, C.-P. (2003). Differential effects of neurotrophins and schwann cell-derived signals on neuronal survival/growth and synaptogenesis. *J. Neurosci.* **23**, 5050-5060. doi:10.1523/JNEUROSCI.23-12-05050.2003

Rauvala, H. and Peng, H. B. (1997). HB-GAM (heparin-binding growth-associated molecule) and heparin-type glycans in the development and plasticity of neuron-target contacts. *Prog. Neurobiol.* **52**, 127-144. doi:10.1016/S0301-0082(97)00007-5

Reist, N. E., Werle, M. J. and McMahan, U. J. (1992). Agrin released by motor neurons induces the aggregation of acetylcholine receptors at neuromuscular junctions. *Neuron* **8**, 865-868. doi:10.1016/0896-6273(92)90200-W

Ruegg, M. A. and Bixby, J. L. (1998). Agrin orchestrates synaptic differentiation at the vertebrate neuromuscular junction. *Trends Neurosci.* **21**, 22-27. doi:10.1016/S0166-2236(97)01154-5

Ruegg, M. A., Tsim, K. W. K., Horton, S. E., Kröger, S., Escher, G., Gensch, E. M. and McMahan, U. J. (1992). The agrin gene codes for a family of basal lamina proteins that differ in function and distribution. *Neuron* **8**, 691-699. doi:10.1016/0896-6273(92)90090-Z

Sanes, J. R. and Yamagata, M. (2009). Many paths to synaptic specificity. *Annu. Rev. Cell Dev. Biol.* **25**, 161-195. doi:10.1146/annurev.cellbio.24.110707.175402

Santiago-Medina, M., Gregus, K. A., Nichol, R. H., O'Toole, S. M. and Gomez, T. M. (2015). Regulation of ECM degradation and axon guidance by growth cone invadosomes. *Development* **142**, 486-496. doi:10.1242/dev.108266

Scotton, P., Bleckmann, D., Stebler, M., Sciandra, F., Brancaccio, A., Meier, T., Stetefeld, J. and Ruegg, M. A. (2006). Activation of muscle-specific receptor tyrosine kinase and binding to dystroglycan are regulated by alternative mRNA splicing of agrin. *J. Biol. Chem.* **281**, 36835-36845. doi:10.1074/jbc.M607887200

Short, C. A., Suarez-Zayas, E. A. and Gomez, T. M. (2016). Cell adhesion and invasion mechanisms that guide developing axons. *Curr. Opin. Neurobiol.* **39**, 77-85. doi:10.1016/j.conb.2016.04.012

Stehbens, S. J., Paszek, M., Pemble, H., Ettinger, A., Gierke, S. and Wittmann, T. (2014). CLASPs link focal-adhesion-associated microtubule capture to localized exocytosis and adhesion site turnover. *Nat. Cell Biol.* **16**, 561-573. doi:10.1038/ncb2975

VanSaun, M., Herrera, A. A. and Werle, M. J. (2003). Structural alterations at the neuromuscular junctions of matrix metalloproteinase 3 null mutant mice. *J. Neurocytol.* **32**, 1129-1142. doi:10.1023/B:NEUR.0000021907.68461.9c

Wu, H., Lu, Y., Shen, C., Patel, N., Gan, L., Xiong, W. C. and Mei, L. (2012). Distinct roles of muscle and motoneuron LRP4 in neuromuscular junction formation. *Neuron* **75**, 94-107. doi:10.1016/j.neuron.2012.04.033

Yang, J.-F., Cao, G., Koirala, S., Reddy, L. V. and Ko, C.-P. (2001). Schwann cells express active agrin and enhance aggregation of acetylcholine receptors on muscle fibers. *J. Neurosci.* **21**, 9572-9584. doi:10.1523/JNEUROSCI.21-24-09572.2001

Yogev, S. and Shen, K. (2014). Cellular and molecular mechanisms of synaptic specificity. *Annu. Rev. Cell Dev. Biol.* **30**, 417-437. doi:10.1146/annurev-cellbio-100913-012953

Yumoto, N., Kim, N. and Burden, S. J. (2012). Lrp4 is a retrograde signal for presynaptic differentiation at neuromuscular synapses. *Nature* **489**, 438-442. doi:10.1038/nature11348

Zhai, R. G., Vardinon-Friedman, H., Cases-Langhoff, C., Becker, B., Gundelfinger, E. D., Ziv, N. E. and Garner, C. C. (2001). Assembling the presynaptic active zone: a characterization of an active one precursor vesicle. *Neuron* **29**, 131-143. doi:10.1016/S0896-6273(01)00185-4

Zhang, B., Luo, S., Wang, Q., Suzuki, T., Xiong, W. C. and Mei, L. (2008). LRP4 serves as a coreceptor of agrin. *Neuron* **60**, 285-297. doi:10.1016/j.neuron.2008.10.006